AFRL-AFOSR-UK-TR-2015-0009

Compact, high-power, fiber-laser-based coherent sources tunable in the mid-infrared and THz spectrum

Majid Ebrahim-Zadeh

ICFO-THE INSTITUTE OF PHOTONIC SCIENCES
AVENIDA CARL FRIEDRICH GAUSS 3
CASTELLDEFELS, BARCELONA, 08860
SPAIN

EOARD GRANT #FA8655-12-1-2128

Report Date: February 2015

Final Report from 15 August 2012 to 13 August 2014

Air Force Research Laboratory
Air Force Office of Scientific Research
European Office of Aerospace Research and Development
Unit 4515, APO AE 09421-4515

REPORT DOCUMENTATION PAGE

Form Approved OMB No. 0704-0188

1. REPORT DATE *(DD-MM-YYYY)*	2. REPORT TYPE	3. DATES COVERED *(From – To)*
20 February 2015	**Final**	**15 August 2012 –13 August 2014**

4. TITLE AND SUBTITLE

Compact, high-power, fiber-laser-based coherent sources tunable in the mid-infrared and THz spectrum

5a. CONTRACT NUMBER

5b. GRANT NUMBER

FA8655-12-1-2128

5c. PROGRAM ELEMENT NUMBER

61102F

6. AUTHOR(S)

Majid Ebrahim-Zadeh

5d. PROJECT NUMBER

5d. TASK NUMBER

5e. WORK UNIT NUMBER

7. PERFORMING ORGANIZATION NAME(S) AND ADDRESS(ES)

ICFO-THE INSTITUTE OF PHOTONIC SCIENCES
AVENIDA CARL FRIEDRICH GAUSS 3
CASTELLDEFELS, BARCELONA, 08860
SPAIN

8. PERFORMING ORGANIZATION REPORT NUMBER

N/A

9. SPONSORING/MONITORING AGENCY NAME(S) AND ADDRESS(ES)

EOARD
Unit 4515
APO AE 09421-4515

10. SPONSOR/MONITOR'S ACRONYM(S)

AFRL/AFOSR/IOE (EOARD)

11. SPONSOR/MONITOR'S REPORT NUMBER(S)

AFRL-AFOSR-UK-TR-2015-0009

12. DISTRIBUTION/AVAILABILITY STATEMENT

Distribution A: Approved for public release; distribution is unlimited.

13. SUPPLEMENTARY NOTES

14. ABSTRACT

In the overall project, we have made substantial progress in the advancement of nonlinear frequency conversion sources and optical parametric oscillators (OPOs) for the deep mid-infrared (mid-IR) spectral regions >5 μm. We have successfully developed tunable deep mid-IR systems in both continuous-wave (cw) and ultrafast femtosecond time-scales using compact fiber lasers and Kerr-lens modelocked Ti:sapphire laser as pump source. In cw operation, we have achieved world-record output powers, while in the ultrafast femtosecond time-scale we have demonstrated world-record broadband wavelength tuning in the deep mid- IR in rapid static geometry using OPO cavity delay tuning.

15. SUBJECT TERMS

EOARD, high-power coherent radiation, intracavity wavelength down-conversion, laser THz sources, MgO:PPLN, MgO:sPPLT, mid-infrared and THz spectrum, non-invasive detection of explosives, THz radiation at milliWatt level, tunable mid-IR and THz sources, ytterbium (Yb) fiber lasers

16. SECURITY CLASSIFICATION OF:			17. LIMITATION OF ABSTRACT	18, NUMBER OF PAGES	19a. NAME OF RESPONSIBLE PERSON
a. REPORT	b. ABSTRACT	c. THIS PAGE			John Gonglewski
UNCLAS	UNCLAS	UNCLAS	SAR	32	19b. TELEPHONE NUMBER *(Include area code)* +44 (0)1895 616007

FINAL REPORT
(20 September 2013 to 20 February 2015)

Project Title:
Compact, high-power, fiber-laser-based coherent sources tunable in the mid-infrared and THz spectrum
(EOARD Award # FA8655-12-1-2128)

Majid Ebrahim-Zadeh[1,2]

[1] ICFO-The Institute of Photonic Sciences, Mediterranean Technology Park, 08860 Castelldefels, Barcelona, Spain
[2] Institucio Catalana de Recerca i Estudis Avancats (ICREA), Passeig Lluis Companys 23, Barcelona 08010, Spain
Tel: 0034-93 553 4047; Fax: 0034-93 553 4000
majid.ebrahim@icfo.es; www.icfo.es

Abstract
In the overall project, we have made substantial progress in the advancement of nonlinear
frequency conversion sources and optical parametric oscillators (OPOs) for the deep mid-infrared (mid-IR) spectral regions >5 μm. We have successfully developed tunable deep mid-IR systems in both continuous-wave (cw) and ultrafast femtosecond time-scales using compact fiber lasers and Kerr-lensmode-locked Ti:sapphire laser as pump source. In cw operation, we have achieved world-record output powers, while in the ultrafast femtosecond time-scale we have demonstrated world-record broadband wavelength tuning in the deep mid-IR in rapid static geometry using OPO cavity delay tuning.

Reports for Years 1 and Years 2, appended below give more detailed breakout of the results of the grant.

Project Title:

Compact, high-power, fiber-laser-based coherent sources tunable in the mid-infrared and THz spectrum

(EOARD Award # FA8655-12-1-2128)

Progress Report, Year 2 (20 February 2015)

Majid Ebrahim-Zadeh[1,2]

[1] *ICFO-The Institute of Photonic Sciences, Mediterranean Technology Park, 08860 Castelldefels, Barcelona, Spain*
[2] *Institucio Catalana de Recerca i Estudis Avancats (ICREA), Passeig Lluis Companys 23, Barcelona 08010, Spain*

Tel: 0034-93 553 4047; Fax: 0034-93 553 4000
majid.ebrahim@icfo.es; www.icfo.es

Abstract

During the second year of the project, we have made substantial progress in the advancement of nonlinear frequency conversion sources and optical parametric oscillators (OPOs) for the deep mid-infrared (mid-IR) spectral regions >5 μm. We have successfully developed tunable deep mid-IR systems in both continuous-wave (cw) and ultrafast femtosecond time-scales using compact fiber lasers and Kerr-lens-mode-locked Ti:sapphire laser as pump source. In cw operation, we have achieved world-record output powers, while in the ultrafast femtosecond time-scale we have demonstrated world-record broadband wavelength tuning in the deep mid-IR in rapid static geometry using OPO cavity delay tuning.

In the cw regime, we have developed a source of tunable radiation in the deep mid-IR, which can provide tens of milliwatts of output power in the 6460-7517 nm spectral range. The source is based on difference-frequency generation (DFG) in orientation-patterned (OP)-GaAs pumped by a Tm-fiber laser at 2010 nm and a 1064 nm-Yb-fiber-pumped cw OPO. Using a 25.7-mm-long OP-GaAs crystal, we have generated up to 51.1 mW of output power at 6790 nm, with >40 mW and >20 mW across 32% and 80% of the mid-infrared tuning range, respectively, which is to our knowledge the highest tunable cw power generated in OP-GaAs in this spectral range. The DFG output at maximum power exhibits passive power stability better than 2.3% rms over more than 1 hour and a frequency stability of 1.8 GHz over more than one minute, in high spatial beam quality. We have also studied the system and crystal performance at high pump powers.

In the high-repetition-rate ultrafast time domain, we have developed the first femtosecond OPO for the deep mid-IR by exploiting the new nonlinear material, $CdSiP_2$ (CSP), pumped by a Kerr-lens-mode-locked (KLM) Ti:sapphire laser in a novel internal cascaded pumping configuration that circumvents the fundamental short-wavelength material absorption in CSP. In this new scheme, the CSP crystal is synchronously pumped internal to a MgO:PPLN femtosecond OPO in a composite cavity geometry. The robust and practical architecture allows access to high intracavity signal intensities in the MgO:PPLN femtosecond OPO to reach oscillation threshold in CSP, while providing the required pump wavelength near ~1 μm to avoid absorption in CSP. Using this approach, we have achieved continuous deep mid-IR wavelength coverage across 5500-8500 nm in a rapid and static geometry by simple cavity delay tuning of CSP OPO at room temperature and with high output stability.

1. Record-power, continuous-wave, fiber-based source tunable in the deep mid-IR based on OP-GaAs

1.1. Introduction

Continuous-wave (cw) laser light sources with extended tunability in the deep mid-IR are of considerable interest for a diverse range of applications, including spectroscopy, trace gas detection, safety and security, as well as medical and biological applications [1-3]. With the scarcity of solid-state lasers, quantum cascade lasers (QCLs) represent viable sources, capable of providing hundreds of mW of cw power in the mid-IR [4]. However, wide tuning together with narrow linewidth remain major limitations. As such, for practical generation of widely tunable cw radiation in the mid-IR, nonlinear optical techniques based on difference-frequency generation (DFG) [2] and optical parametric oscillators (OPOs) [5] still represent a highly effective approach for the development of viable mid-IR coherent sources. The cw OPOs based on MgO:PPLN are now firmly established as the most effective approach for the generation of tunable high-power radiation up to ~4 μm [6], with wavelengths up to 5 μm also obtained at mW power level [7]. However, the intrinsic onset of absorption in MgO:PPLN and other oxide-based ferroelectric materials beyond ~4 μm presents a fundamental barrier to wavelength generation at practical powers further into the mid-IR. As such, the search for alternative nonlinear materials with high transmission above ~4 μm and effective techniques for spectral expansion into the longer mid-IR wavelengths must be explored.

In this context, orientation-patterned (OP)-GaAs is a highly attractive nonlinear crystal. Its high nonlinear coefficient ($d_{eff}=d_{14}$~94 pm/V) [8], wide transparency across 0.9-17 μm, high thermal conductivity (46 W/mK), and high damage threshold [9] make it a primary candidate for deep mid-IR generation. Its nonlinear figure of merit, $F=d_{eff}^2/n^3$ (n is the refractive index), is nearly ten times that of MgO:PPLN. In an early report, a pulsed OPO based on OP-GaAs, tunable in the 5.7-9.1 μm range was demonstrated, using a PPLN OPO pumped by a Q-switched Nd:YAG laser at 1064 [10]. Recently, a pulsed OP-GaAs OPO tunable over 8.8-11.5 μm was reported using direct pumping with a Q-switched Tm,Ho:YLF laser [11]. However, the development of cw OPOs at wavelengths >4 μm still remains a major challenge, in a large part due to the high threshold sensitivity to cavity loss in practical singly-resonant configuration, combined with the difficulty in achieving relatively complex mirror and crystal coatings of high quality and low loss in the deep mid-IR spectral range to achieve oscillation threshold. In the meantime, one can circumvent this obstacle by deploying the alternative technique of DFG, which is single-pass and does not require the attainment of an oscillation threshold. The technique can provide an effective and robust approach for the generation of non-negligible output powers at longer wavelengths [2]. In the past few years, DFG based on OP-GaAs, with cw output powers up to several mW has been demonstrated [12]. A few years ago, a cw source tunable across 7.6-8.2 mm with sub-mW output power was reported by using DFG between an Er-doped fiber source and a Tm-doped fiber laser in OP-GaAs [13]. Although these sources provide coverage across an important spectral range of interest in the deep mid-IR, the attainment of high output power, leading to noise-free, pure spectral output is yet to be demonstrated. As part of this project, we are able to report the generation of multi-tens of mW level output power in the spectral range of 6.4-7.5 μm by exploiting DFG between a high-power Yb-fiber-pumped cw OPO and a cw Tm-fiber laser in OP-GaAs. Today, cw OPOs based on MgO:PPLN are well established as practical and reliable sources of tunable radiation in the mid-IR capable of delivering watt-level output power across 2-4 μm [6,14]. With further advances in fiber laser technology, high-power cw Tm-fiber lasers at ~2 μm are also now becoming commercially available with improving performance for nonlinear frequency conversion [15]. Hence, the combination of tunable watt-level cw MgO:PPLN OPOs and high-power Tm-fiber lasers can be effectively exploited to achieve wavelength generation into the deep mid-IR at practical powers, and with wide tunability, using the DFG technique. By deploying such a scheme in OP-GaAs, we have generated cw radiation across 6460-7517 nm, with as much as 51.1 mW of output power at 6790 nm and >40 mW across 32% of tuning range, in TEM_{00} spatial mode profile, with good power and frequency stability. To our knowledge, these are the highest cw power generated with OP-GaAs, with broad tunability in the deep mid-IR.

1.2. Experimental Setup

The schematic of the experimental setup is shown in Fig. 1.1. The first pump source used is a commercial cw Tm-fiber laser (IPG Photonics, TLR-50-2010-LP), delivering up to 43 W of output power at 2010 nm in a linearly-polarized beam with a quality factor of M^2=1.2. The linewidth of the laser, measured using an optical spectrum analyser with a resolution of 0.1 nm, is ~1.5 nm. The second pump source is a home-built cw OPO based on an earlier design [6], but using a 38-mm-long MgO:PPLN crystal pumped by a commercial cw Yb-fiber laser (IPG Photonics, YLR-30-1064-LP-SF) at 1064 nm. The OPO is singly-resonant for the signal, and provides tunable output across 2.4-2.9 μm in the non-resonant idler, with as much as 4.9 W of cw power at λ_i=2748 nm for grating period of $\Lambda_{MgO:PPLN}$=31.5 μm. The OPO signal linewidth at λ_s=1683.9 nm, measured using an optical spectrum analyser, is $\Delta\lambda_s$=0.9 nm, limited by the instrument resolution. However, given the single-frequency nature of the cw Yb-fiber pump laser ($\Delta\lambda$~89 kHz), the generated signal and idler are also both expected to be single-frequency. The Tm-fiber laser is operated at maximum power, and the input power, P_1, for DFG is adjusted using a combination of a half-wave plate (H_1) and a polarizing beam-splitter (PBS). A second half-wave plate (H_2) is used to control the pump polarization for phase-matching in the DFG crystal. The output power from the OPO, P_2, is adjusted by varying the Yb-fiber pump power using a combination of a half-wave plate and a polarizing beam-splitter cube [6]. For DFG, we used 25.7-mm-long, 9-mm-wide, 2.1-mm-thick OP-GaAs crystal with grating period of $\Lambda_{OP\text{-}GaAs}$=63.5 μm.[1] The crystal has antireflection (AR)-coated end-faces over 2000-8000 nm (R<18%) and is housed in an oven with stability of ±0.1 °C, which can be controlled from room temperature to 200 °C. The pump beams, P_1 and P_2, are both *e*-polarized, allowing type 0 (*ee*→*e*) phase-matching for DFG in the OP-GaAs crystal. The lenses, $L_{1,2}$ and $L_{3,4}$, are used to adjust the beam diameters, while mirrors $M_{2,3}$ and $M_{4,5}$ are used to optimize spatial overlap of the two beams, P_1 and P_2, on lens, L_5, respectively. Mirror, M_5, is reflective (R>90%) for P_2, while highly transmitting (T>99%) for P_1. The lens, L_5, of focal length, f=300 mm, is used to focus P_1 and P_2 to waist radii of w_1~49 μm and w_2~62 μm, corresponding to confocal focussing parameters of ξ_1=1.02 and ξ_2=0.92, respectively, at the centre of the OP-GaAs crystal (b_1~b_2). Dichroic mirror, M_6, is used to separate P_1, while filter F_1 is used to separate P_2, from the generated DFG beam. To reject any residual P_1 and P_2 from the DFG output power, we used an additional filter, F_2.

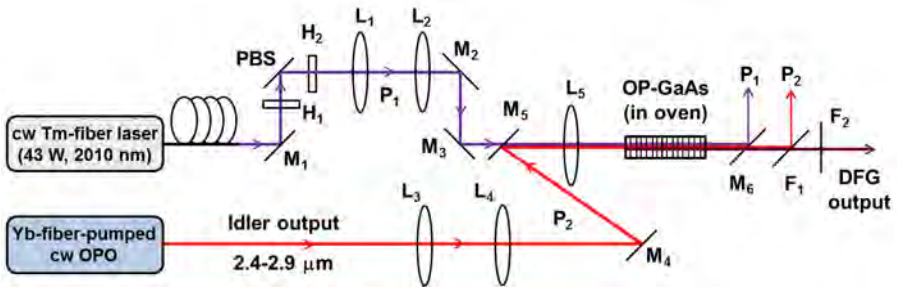

Fig. 1.1. Schematic of the experimental setup. PBS, polarizing beam-splitter; $H_{1,2}$, half-wave plates; $L_{1\text{-}4}$, lens; $M_{1\text{-}6}$, mirrors; $F_{1,2}$, filters.

1.3. Results and Discussion

The DFG spectral tuning in the mid-IR in the present device was achieved by tuning the OPO idler wavelength. To study the DFG tuning range, we varied the temperature of the MgO:PPLN crystal, T_{OPO}, and simultaneously adjusted the phase-matching temperature, T_{DFG}, of the OP-GaAs crystal, at maximum pump powers. By varying T_{OPO} from 40 °C to 105 °C, and T_{DFG} from 38.5 ºC to 190.5 ºC, we were able to achieve DFG tuning across 6460-7517 nm. Figure 1.2(a) shows the measured DFG wavelengths using a wavemeter (*Bristol 721* Spectrum Analyser) with absolute accuracy of ±1 ppm for mid-IR, and the calculated values using energy conservation (ν_1-ν_2=ν_{DFG}, where ν_1, ν_2 and ν_{DFG} are the frequencies of Tm-fiber, OPO idler, and DFG output, respectively), as a function of OPO idler wavelength. As evident from the plot, we were able to obtain continuous DFG spectral coverage over ~1050 nm by tuning the OPO idler wavelength over only ~170 nm. Figure 1.2(b) shows the measured DFG tuning

[1] *The OP-GaAs crystal was supplied by BAE Systems, Inc., Nashua, New Hampshire 03061-0868, USA.*

range, together with the calculated curve using the Sellmeier equations for OP-GaAs [16], as a function of the crystal temperature. The slight discrepancy in the DFG phase-matching temperature is attributed to the heating of the OP-GaAs crystal at higher input pump powers.

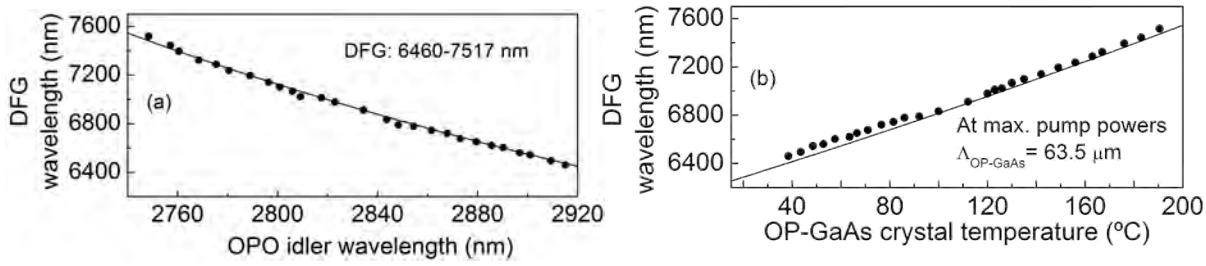

Fig. 1.2. Measured (filled circle) and calculated (solid line) (a) DFG tuning range across the OPO idler wavelength, and (b) DFG wavelength versus the OP-GaAs crystal temperature.

We measured the generated DFG output power across the mid-IR for a fixed available Tm-fiber laser power of 36.7 W, and fixed maximum OPO idler power at any given idler wavelength at the input to the OP-GaAs crystal. The results are shown in Fig. 1.3, where it can be seen that the generated DFG was continuously tunable across the entire 6460-7517 nm range, providing >40 mW and >20 mW over 32% and 80% of the full DFG spectral coverage, respectively, with a maximum of 51.1 mW at λ_{DFG}=6790 nm. The data correspond to the generated power at the exit face of the OP-GaAs crystal, after correction for a total transmission loss of ~20% through the dichroic mirror, M_6, and the two filters, F_1 and F_2. The drop in the DFG power at the centre of the tuning range is due to the corresponding drop in the OPO idler power, owing to the maximum absorption coefficient of the OH-vibration peak at 2826 nm in the MgO:PPLN crystal [17]. The inset of Fig. 1.3 shows the corresponding maximum OPO idler power available for DFG across the tuning range. The DFG power across the tuning range follows a similar behaviour to the input OPO idler power, except at longer DFG wavelengths. This is attributed to the increased reflectivity of the AR coating on the OP-GaAs crystal, as well as reduced transmission of dichroic mirror, M_5, at longer DFG wavelengths.

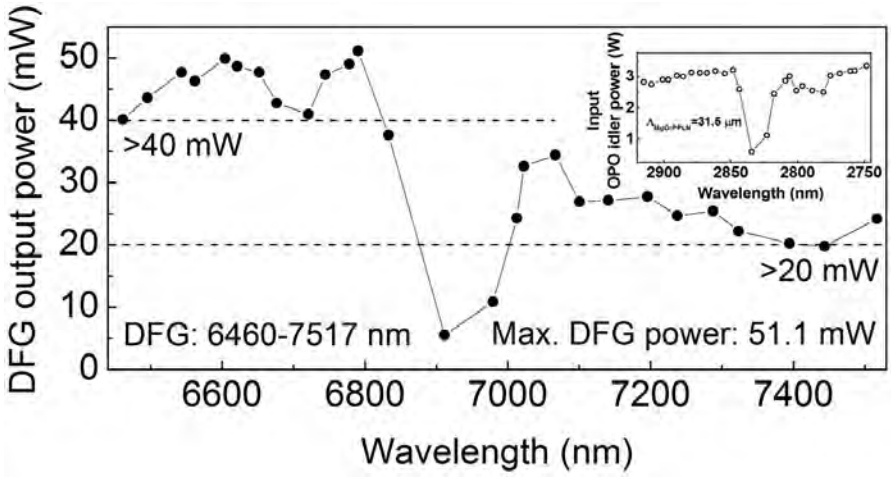

Fig. 1.3.Variation of DFG power across the tuning range, at maximum pump powers. Inset: Corresponding input OPO idler power available for DFG across the tuning range.

To further investigate the performance of the mid-IR cw DFG device, we performed power scaling measurements, while maintaining one of the input pump powers fixed at the maximum. Keeping the Tm-fiber power fixed at 36.7 W, and increasing the OPO idler power by increasing the Yb-fiber pump power, we recorded the DFG output power at λ_{DFG}=6543 nm as a function of input OPO idler power. The result is shown in Fig. 1.4(a). The DFG power increases linearly with the input OPO idler power, reaching as high as 47.6 mW. While performing the power scaling measurement, T_{DFG} was adjusted as the OPO idler power was varied, because of the change in the OPO idler wavelength with the increase in the Yb-fiber pump power. As shown in the inset of Fig. 1.4(a), T_{DFG} increases from 45 ºC to 48.5 ºC with the increase in the input OPO idler power to maximum, while the idler wavelength

simultaneously decreases from 2910.5 nm to 2900.9 nm. We then recorded the variation of DFG output power with the increase in Tm-fiber power, while keeping the OPO idler power fixed at the maximum value of 2.9 W at λ_i=2901 nm. The result is shown in Fig. 1.4(b). As evident, the DFG output power has a similarly linear dependence on the Tm-fiber pump power. While increasing the laser pump power, T_{DFG} was adjusted to generate maximum DFG power at λ_{DFG}=6543 nm. As shown in the inset of Fig. 1.4(b), T_{DFG} decreases from 51.7 ºC to 48.5 ºC, with the increase in the Tm-fiber pump power, due to the heating of the OP-GaAs crystal at high pump powers. We also investigated stronger and looser focusing for both beams, P_1 and P_2, with smaller beam waist radii (w_1~35 μm, w_2~45 μm) and larger beam waist radii (w_1~88 μm, w_2~110 μm), respectively, at the center of the OP-GaAs crystal, by changing the focal length of lens, L_5. However, this resulted in lower DFG output power, which could be due to the reduced spatial overlap of P_1 and P_2 beams within the OP-GaAs crystal.

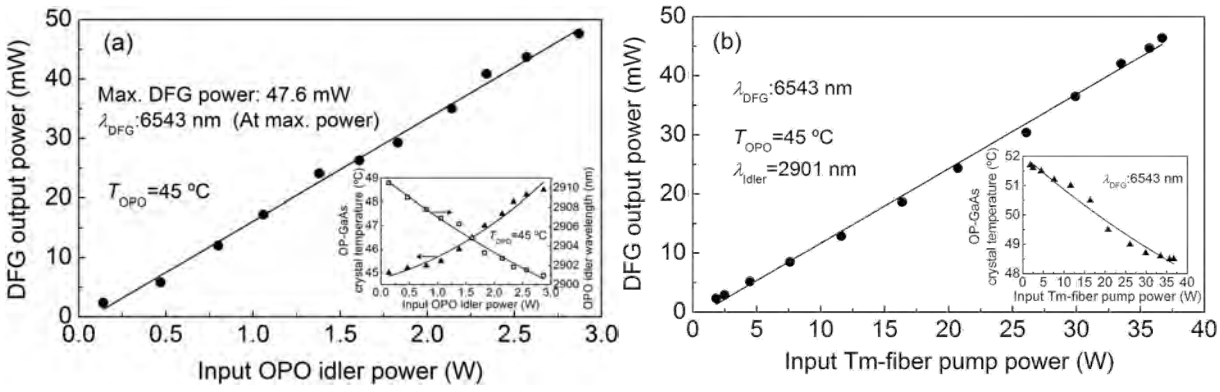

Fig. 1.4. Dependence of the measured cw DFG power at 6543 nm on (a) Incident OPO idler power, and (b) Incident Tm-fiber pump power. Solid lines are guide to the eye. Insets: (a) OP-GaAs quasi-phase-matched temperature and the corresponding OPO idler wavelength, as a function of OPO idler power. (b) OP-GaAs crystal temperature as a function of laser pump power at λ_{DFG}=6543 nm. Solid lines are guide to the eye.

We then recorded the passive power stability of the DFG output at 6604 nm at the maximum input pump powers, under free-running conditions. The result is shown in Fig. 1.5, where the generated mid-IR power is recorded to exhibit a passive stability better than 2.3% rms over >1 hour. The instability in power is attributed to the mechanical vibrations and air currents in the laboratory and possible mode-hopping in the OPO in the absence of active stabilization. The DFG power stability is expected to be improved with active control of the OPO, as well as thermal and mechanical-vibration isolation of the system. The inset of Fig. 1.5 shows the near-field energy distribution of the mid-IR output beam at 6604 nm, at maximum pump powers, recorded using Pyrocam III camera. The result confirms excellent spatial quality with a beam circularity >95%. Similar profiles were obtained across the entire DFG tuning range. Moreover, we have not observed any degradation in the beam quality, nor damage to the OP-GaAs crystal or the AR coating, after sustained long-term operation.

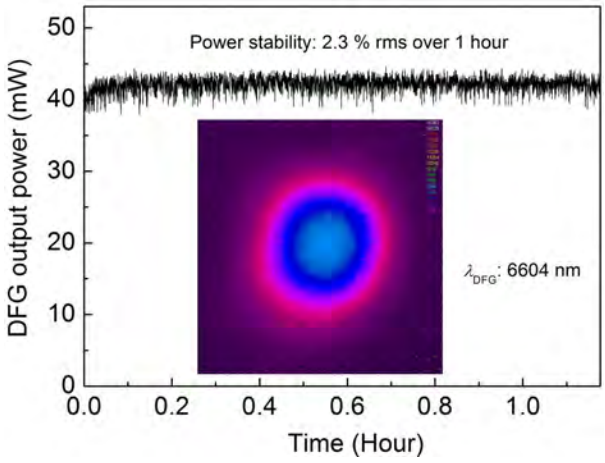

Fig. 1.5. DFG output power stability at maximum power over more than 1 hour. Inset: Near-field TEM_{00} energy distribution of the generated DFG beam.

We also investigated the frequency stability of the generated cw mid-IR radiation by recording the DFG frequency as a function of time using wavemeter (Bristol 721) at maximum power. The result is shown in Fig. 1.6. Under free-running conditions and in the absence of thermal isolation, the DFG output exhibits a peak-to-peak frequency deviation of $\Delta\nu_{DFG}$=1.8 GHz over >1 minute, with a central wavelength of 6590.1494 nm. With better isolation of the system, and active stabilization of OPO and Tm-fiber laser wavelength, further improvements in the frequency stability of the mid-IR output are expected. Also shown in the inset of Fig. 1.6 is the DFG spectrum at λ_{DFG}=6604 nm measured using spectrum analyser (Bristol 721), with spectral resolution of 6 GHz in the mid-IR. As can be seen, the spectrum has a FWHM linewidth of 4.5 nm (~30 GHz). The measured frequency stability also indicates the narrow linewidth of the DFG output.

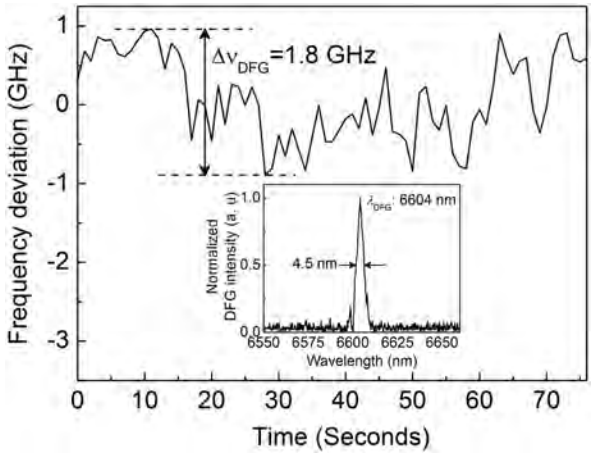

Fig. 1.6. Frequency stability of DFG output at maximum power over more than 60 seconds. Inset: DFG spectrum showing a linewidth of 4.5 nm.

2. Record-tuning, intracavity-cascaded, femtosecond optical parametric oscillator for the deep mid-IR based on $CdSiP_2$

2.1. Introduction

With the scarcity of ultrafast solid-state lasers, synchronously-pumped OPOs offer a viable approach to the generation of ultrashort pulses in the mid-IR. By exploiting oxide-based birefringent nonlinear materials such as $LiNbO_3$, $KTiOPO_4$, $RbTiOAsO_4$ and $LiTaO_3$, and their quasi-phase-matched (QPM) counterparts, PPLN, PPKTP, PPRTA and PPLT, a variety of femtosecond OPOs pumped by the Kerr-lens-mode-locked (KLM) Ti:sapphire laser have been realized covering spectral regions from ~250 nm in UV up to ~4.5 μm in mid-IR [18]. On the other hand, access to deep-IR wavelengths beyond ~4.5 μm in oxide-based crystals is fundamentally limited by multiphonon absorption, placing a practical upper limit of ~4 μm to tuning coverage in all such OPOs. As an alternative, non-oxide QPM materials, such as OP-GaAs, can be used for wavelength generation beyond ~4 μm, as described in Section 1, but this requires pump sources above ~2 μm to avoid two-photon absorption. Chalcopyrite crystals such as $AgGaSe_2$, $AgGaS_2$, and the most developed $ZnGeP_2$, can generate deep mid-IR radiation up to ~10 μm, but must be pumped above ~1 μm to avoid two-photon and residual absorption, and material quality still remains a major practical limitation yet to be overcome. In an effort to extend the wavelength reach of Ti:sapphire-pumped femtosecond OPOs beyond ~4 μm, external cascaded pumping using two OPOs in series, based on $CsTiOAsO_4$ and $AgGaS_2$, was previously deployed, providing tuning coverage up to ~8 μm [19]. However, such external tandem pumping schemes result in relatively complex architectures involving two OPO cavities synchronized in series to one another, and to the pump laser, leading to increased output instabilities, which are not desirable for many practical applications.

The new nonlinear material, $CdSiP_2$ (CSP), has the important capability to generate radiation beyond ~6 μm under noncritical phase-matching (NCPM) at room temperature with direct pumping at ~1 μm [20]. Using CSP, a number of ultrafast parametric sources have been recently demonstrated by deploying mode-locked solid-state and fiber pump lasers at ~1 μm, providing spectral coverage from ~6.1 to ~6.7 μm [21-23]. However, the development of ultrafast OPOs based on CSP using the KLM Ti:sapphire laser, the workhorse of ultrafast technology, is precluded by the short-wavelength cutoff below ~1 μm in this material. Here, we report the first OPO for the deep mid-IR based on CSP pumped by a KLM Ti:sapphire laser using a novel internal cascaded scheme that circumvents the fundamental short-wavelength material absorption. In this new scheme, the CSP is synchronously pumped internal to a MgO:PPLN femtosecond OPO in a composite cavity geometry. The robust and practical architecture allows access to high intracavity signal intensities in the MgO:PPLN OPO to reach oscillation threshold in the CSP OPO, while providing the required pump wavelength near ~1 μm to avoid absorption in CSP. Using this approach, we have achieved continuous deep-IR wavelength coverage across ~6-8 μm in a rapid and static geometry by simple cavity delay tuning of CSP OPO at room temperature and with high output stability.

2.2. Experimental Setup

The schematic of the experimental setup is shown in Fig. 1. The KLM Ti:sapphire laser provides an average power of 900 mW at 796 nm ~155 fs pulses with a 7-nm bandwidth at 76 MHz for synchronous pumping the intracavity-cascaded OPO (IC-OPO). The IC-OPO is arranged in a composite bifocal standing-wave cavity comprising a primary OPO based on a 500-μm-long MgO:PPLN, and a secondary OPO based on a 500-μm-long CSP crystal. The MgO:PPLN crystal incorporates fanned gratings with periods of Λ=16-23 μm. The CSP crystal is cut at θ=45° (ϕ=0°) for type I (*e*→*oo*) NCPM.[2] The primary OPO is formed by concave mirrors, M1-M4 (*r*=100 mm), and plane mirrors, M5 and M7. The secondary OPO is formed by mirrors, M1-M4 and M7, but with plane mirror, M6, completing the cavity. All mirrors are broadband high reflectors (*R*>99.8%) over 980-1640 nm wit high transmission (*T*>90%) over 710-840 nm, ensuring singly-resonant signal oscillation in both OPOs. A prism pair is deployed in one arm of the cavity for group delay dispersion (GDD) compensation. The two cavities are separated by a thin-film-polarizer (TFP) and synchronized to the pump laser by placing M5 and M6 on separate translation stages for fine-adjustment of the resonator lengths and independent cavity delay tuning. The TFP is highly reflecting (*R*>99%) over 1000-1100 nm and highly transmitting (*T*>98%) over 1150-1350 nm for both *e* and *o* polarizations. A lens *L* (*f*=8 cm) is used to focus the pump beam to a waist radius, w_0=25 μm, inside the MgO:PPLN crystal. A half-wave plate provides *e* pump polarization for type 0 (*e*→*ee*) phase-matching in the MgO:PPLN crystal. The generated signal pulses from the MgO:PPLN OPO are ~210 fs with a bandwidth of ~7.3 nm, and, in turn, provide the *e* polarization to pump the CSP OPO under type I (*e*→*oo*) NCPM. A photograph of the IC-OPO in oscillation, showing the CSP crystal, is included in the inset of Fig. 2.1.

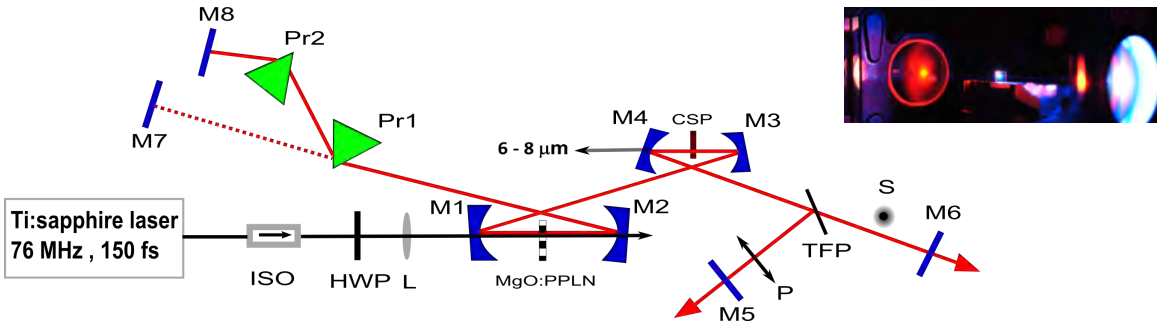

Fig. 2.1. Schematic of the Ti:sapphire-pumped intracavity-cascaded femtosecond OPO based on MgO:PPLN and CSP for the generation of tunble radiation in the 6-8 μm range. ISO: Faraday Isolator, HWP: Half-wave-plate, L: Lens, M1-8: Highly reflecting mirrors, Pr1-2: Prism pair, TFP: Thin-film polarizer. Inset: Photograph of the IC-SPOPO in oscillation showing the CSP at room temperature.

[2] *The $CdSiP_2$ crystal was supplied by BAE Systems, Inc., Nashua, New Hampshire 03061-0868, USA.*

2.3. Results and Discussion

We achieved successful operation of the IC-OPO at 600 mW of average Ti:sapphire input pump power. Fig. 2.2(a) shows the simultaneous oscillation of the signal in MgO:PPLN OPO and CSP OPO when successful operation of the IC-OPO is established. Under this condition, a pump depletion of 20% is recorded, as shown in Fig. 2.2(b). The signal spectra generated by the CSP femtosecond OPO with the center wavelength tunable across 1170–1235 nm are shown in Fig. 2.2(c). The tuning was achieved only via cavity length variation of CSP OPO over ΔL~70 μm by translating mirror, M6. The spectra were obtained at a MgO:PPLN signal wavelength of 1024 nm.

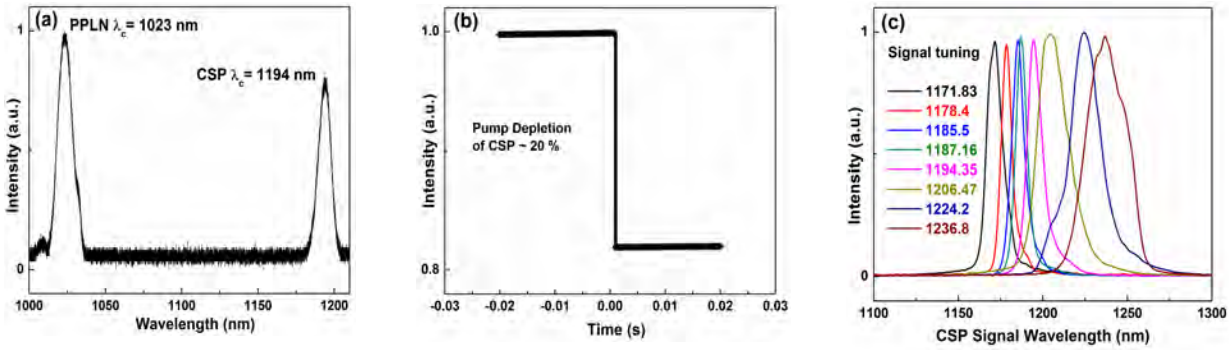

Fig. 2.2 (a) Simultaneous signal oscillation in MgO:PPLN and CSP OPO. (b) Pump depletion, and (c) Signal tuning and spectra with CSP OPO cavity delay.

The corresponding idler spectra are shown in Fig. 2.3(a), representing a tuning range from a center wavelength of 5947 to 8109 nm, with the spectra extending across ~5500-8500 nm. Thus, for a signal tuning range of only ~65 nm, we achieve continuous idler tuning extending over as wide as ~3000 nm just by cavity delay tuning at room temperature, with tuning range limited by the coating of CSP crystal. This is a record deep-IR tunability in CSP to date. Figure 2.3(b) shows the the signal and idler tuning as a function of CSP OPO cavity delay, including the variation in signal power, which reaches a value of 350 μW at zero detuning (ΔL~0). The corresponding idler power was measured to be 64 μW, limited by the low average power of the available KLM Ti:sapphire laser. With a ~5% output coupler in place of M6, we were abale to generate 9 mW of average signal power from the CSP femtoseocnd OPO. Because of the composite cavity design, the IC-OPO exhibits excellent passive stability, as shown in Fig. 2.3(c), with the deep-IR idler power exhibiting a peak-to-peak fluctuation <6% over 2 hours in the absence of thermal and mechanical isolation and electronic stabilization. Also shown is the meaurement of the mid-IR idler beam quality, confirming a near-Gaussian spatial profile.

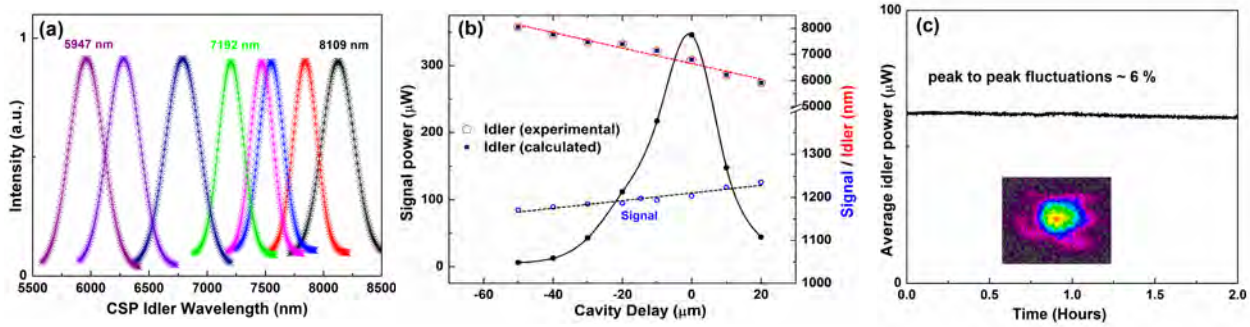

Fig. 2.3 (a) Idler tuning and spectra in the deep mid-IR, (b) Signal/idler wavelength tuning and output power with cavity delay, (c) Idler power stability and spatial beam profile in the deep mid-IR.

3. Conclusions and Future Outlook

In conclusion, we have developed two new sources of tunable radiation coherent in the deep mid-IR, in cw and high-repetiton-rate femtosecond time scale, providing world record performance with regard to output power and wavelength tuning. The demonstrated sources are based on nonlinear frequency conversion techniques of DFG and OPO and exploit compact fiber laser technology and KLM Ti:sapphire laser as the pump source in combination with newly developed materials of OP-GaAs and $CdSiP_2$ as the nonlinear gain crystal.

In the cw regime, we have developed a tunable source of cw radiation for the mid-IR, providing multi-tens of mW output power in the 6460-7517 nm spectral range, for the first time to our knowledge. To achieve such high powers, together with broad tuning range, we have exploited single-pass DFG between a high-power cw Tm-fiber laser and a cw OPO in OP-GaAs. The system provides up to 51.1 mW of cw power in the deep mid-IR, in high beam quality, with good passive power and frequency stability. The output power can be further increased with higher cw OPO idler powers using a longer (~80 mm) MgO:PPLN crystal, and improved AR-coatings on the OP-GaAs crystal. Given the great interest in the wavelength regions of 4-6 μm and 8-12 μm, the atmospheric transmission window for safety and security applications, by using an OP-GaAs crystal with grating periods of ~57 μm and ~69 μm, and OPO idler wavelengths across 3.08-3.96 μm and 2.58-2.72 μm, the obtained tuning range can be further extended to 4.0-5.7 μm and 7.7-9.0 μm, respectively, using the same cw Tm-fiber laser at 2010 nm. With thermal and mechanical isolation, and electronic control of the OPO pump source, the power and frequency stability of the DFG output can be further enhanced. These features make the device a promising source of tunable cw radiation in the deep-mid-IR for a variety of applications. With a view to further scaling to higher powers and furterh wavelegnth expansion in the mid-IR, we are also currently undertking the design and development of a cw OPO based on OP-GaAs pumped directly by the Tm-fiber laser at 2010 nm available in our laboratory. We expect this cw OPO will be able to deliver 100 mW to W-level output powers across the mid-IR, including the important spectral range of 4-5 μm for safety and security applications. We are further exploring the viability of new nonlinear materials such as OP-GaP for the development of cw OPOs for the generation of high-power cw radiation in the 3-8 μm spectral range using the Yb-fiber laser at 1064 nm as the pump source.

In the ultrafast, time domain, we have developed a new source of high-repeptioton-rate femtosecond pulses with record tuning in the deep mid-IR based on a synchronuly-pumped OPO in a novel geometry. The device exploits a novel internal cascaded pumping technique combining a MgO:PPLN and CSP in a composite cavity arrangement, thus circumventing the short-wavelegnth absorption cutoff in the CSP crystal. Using this technique, we have achieved a record spectral coverage in the deep mid-IR with rapid wavelegnth tuning across 5500-8500 nm only by cavity length delay. Because of the novel composite cavity design, the mid-IR output power from the OPO is characterized by high peak-to-peak power stability of ~6% over 2 hours without any environemtnal isolation or active stabilization. The mid-IR idler output is also in high beam quality with near-Gaussian beam profile. Further enhancements in the perofrmance of the OPO with regard to output power scaling are currently underway using a hihg-power KLM femtosecond Ti:sapphire laser, where we expect to geneerate average powers of 10-100 mW in the deep mid-IR. The demonstrated technique is universal and can be extended to all time-scales and other widely available laser pump sources, overcoming the fundamental short-wavelength pump absorption in narrow-bandgap materials for deep-IR generation using OPOs. As such, the development of a compact high-power picosecond OPO for the deep mid-IR based on the cascaded intracavity concept pumped by an Yb-fiber laser is currently underway, with the goal of genrating 100s of mW to W-level ouptut power in the 4-8 μm spectral range.

References

1. A. Elia, C. Di Franco, P. M. Lugara, and G. Scamarcio, "Photoacoustic spectroscopy with quantum cascade lasers for trace gas detection," Sensors 6, 1411-1419 (2006).
2. W. Chen, J. Cousin, E. Poullet, J. Burie, D. Boucher, X. Gao, M. W. Sigrist, and F. K. Tittel, "Continuous-wave mid-infrared laser sources based on difference frequency generation," C. R. Physique 8, 1129-1150 (2007).
3. C. E. Webb and J. D. C. Jones, "Handbook of Laser Technology and Applications: Applications," CRC Press (2004).
4. F. Capasso, "High-performance midinfrared quantum cascade lasers," Optical Engineering 49, 111102 (2010).
5. M. Ebrahim-Zadeh and I. T. Sorokina (eds.), "Mid-Infrared Coherent Sources and Applications," 347–375 (Springer 2008).
6. S. Chaitanya Kumar, R. Das, G. K. Samanta, and M. Ebrahim-Zadeh, "Optimally-output-coupled, 17.5 W, fiber-laser-pumped continuous-wave optical parametric oscillator," Appl. Phys. B 102, 31–35 (2011).
7. M. M. J. W. van Herpen, S. E. Bisson, and F. J. M. Harren, "Continuous-wave operation of a single-frequency optical parametric oscillator at 4–5 mm based on periodically poled $LiNbO_3$," Opt. Lett. 28, 2497-2499 (2003).
8. T. Skauli, K. L. Vodopyanov, T. J. Pinguet, A. Schober, O. Levi, L. A. Eyres, M. M. Fejer, J. S. Harris, B. Gerard, L. Becouarn, E. Lallier, and G. Arisholm, "Measurement of the nonlinear coefficient of orientation-patterned GaAs and demonstration of highly efficient second-harmonic generation," Opt. Lett. 27, 628-630 (2002).
9. A. Grisard, E. Lallier, and B. Gérard Grisard, "Quasi-phase-matched gallium arsenide for versatile mid-infrared frequency conversion," Opt. Materials Express 2, 1020-1025 (2012).
10. K. L. Vodopyanov, O. Levi, P. S. Kuo, T. J. Pinguet, J. S. Harris, M. M. Fejer, B. Gerard, L. Becouarn, and E. Lallier, "Optical parametric oscillation in quasi-phase-matched GaAs," Opt. Lett. 29, 1912-1914 (2004).
11. R. K. Feaver, R. D. Peterson, and P. E. Powers, "Longwave-IR optical parametric oscillator in orientation-patterned GaAs pumped by a 2 mm Tm,Ho:YLF laser," Opt. Express 21, 16104-16110 (2013).
12. S. E. Bisson, T. J. Kulp, O. Levi, J. S. Harris, and M. M. Fejer, "Long-wave IR chemical sensing based on difference frequency generation in orientation-patterned GaAs," Appl. Phys. B 85, 199–206 (2006).
13. S. Vasilyev, S. Schiller, A. Nevsky, A. Grisard, D. Fave, E. Lallier, Z. Zhang, A. J. Boyland, J. K. Sahu, M. Ibsen, and W. A. Clarkson, "Broadly tunable single-frequency cw mid-infrared source with milliwatt-level output based on difference-frequency generation in orientation-patterned GaAs," Opt. Lett. 33, 1413-1415 (2008).
14. K. Devi, S. Chaitanya Kumar, A. Esteban-Martin, and M. Ebrahim-Zadeh, "Antiresonant ring output-coupled continuous-wave optical parametric oscillator," Opt. Express 20, 19313-19321 (2012).
15. K. Devi, S. Chaitanya Kumar, and M. Ebrahim-Zadeh, "13.1 W, high-beam-quality, narrow-linewidth continuous-wave fiber-based source at 970 nm," Opt. Express 19, 11631-11637 (2011).
16. T. Skauli, P. S. Kuo, K. L. Vodopyanov, T. J. Pinguet, O. Levi, L. A. Eyres, J. S. Harris, M. M. Fejer, B. Gerard, L. Becouarn, and E. Lallier, "Improved dispersion relations for GaAs and applications to nonlinear optics," J. Appl. Phys. 94, 6447-6455 (2003).
17. J. M. Cabrera, J. Olivares, M. Carrascosa, J. Rams, R. Müller, and E. Diéguez, "Hydrogen in lithium niobate," Adv. Phys. 45, 349-392 (1996).
18. M. Ebrahim-Zadeh, in *Solid-State Mid- Infrared Laser Sources*, Springer-Verlag Science Series, *Topics Appl. Phys.* 89, (2003).
19. S. Marznell, R. Beigang, and R. Wallenstein, *Appl. Phys. B* 69, 423 (1999).
20. K. T. Zawilski, P. G. Schunemann, T. M. Pollak, D. E. Zelmon, N. C. Fernelius, and F. K. Hopkins, *J. Cryst. Growth* 312, 1127 (2010).
21. S. C. Kumar, A. Agnesi, P. Dallocchio, F. Pirzio, G. Reali, K. Zawilski, P. Schunemann, M. Ebrahim-Zadeh, Opt. Lett. 36, 3236 (2011).
22. S. C. Kumar, M. Jelínek, M. Baudisch, K. Zawilski, P. Schunemann, V. Kubeček, J. Biegert, M. Ebrahim-Zadeh, *Opt. Exp.* 20, 15703 (2012).
23. Z. Zhang, D. T. Reid, S. C. Kumar, M. Ebrahim-Zadeh, P. G. Schunemann, K. T. Zawilski, C. R. Howle, *Opt. Lett.* 38, 5110 (2013).

Publications:

Our efforts during the second year of the project, have resulted in the the following publications, with due acknowledgement to EOARD for their valuable support:

Journal papers

1. **(Invited Paper)** M. Ebrahim-Zadeh, S. Chaitanya Kumar, "Yb-fiber-laser-pumped ultrafast frequency conversion sources from the mid-infrared to the ultraviolet", Special Issue: Progress in Solid State, Fiber, and Tunable Systems (PSSFTS), *IEEE J. Sel. Top. Quantum Electron*. 20, 7600519, 1-19 (2014).
2. **(Invited Paper)** M. Ebrahim-Zadeh, S. Chaitanya Kumar, K. Devi "Yb-fiber-laser-pumped continuous-wave frequency conversion sources from the mid-infrared to the ultraviolet", Special Issue: Progress in Solid State, Fiber, and Tunable Systems (PSSFTS), *IEEE J. Sel. Top. Quantum Electron*. 20, 0902823, 1-23 (2014).
3. K. Devi, P. G. Schunemann, M. Ebrahim-Zadeh, "Continuous-wave, multimilliwatt, mid-infrared source tunable across 6.4-7.5 μm based on orientation-patterned GaAs", *Opt. Lett.* 39, 6751-6754 (2014).
4. **(With Nobel Laureate)** S. Chaitanya Kumar, A. Esteban-Martin, T. Ideguchi, M. Yan, S. Holzner, T. W. Hänsch, N. Picqué, M. Ebrahim-Zadeh, "Few-cycle, broadband, mid-infrared optical parametric oscillator pumped by a 20-fs Ti:sapphire laser", *Laser & Photon. Rev.* 8, L86-L91 (2014).
5. G. K. Samanta, S. Chaitanya Kumar, A. Aadhi, M. Ebrahim-Zadeh, "Yb-fiber-laser-pumped, high-repetition-rate picosecond optical parametric oscillator tunable in the ultraviolet", *Opt. Express* 22, 11476-11487 (2014).
6. V. Ramaiah-Badarla, S. Chaitanya Kumar, M. Ebrahim-Zadeh, "Fiber-laser-pumped, dual-wavelength, picosecond optical parametric oscillator", *Opt. Lett.* 39, 2739-2742 (2014).
7. K. Devi, S. Chaitanya Kumar, A. Esteban-Martin, M. Ebrahim-Zadeh, "Tunable, dual-wavelength interferometrically coupled continuous-wave parametric source", *Appl. Phys. B* 114, 307–312 (2014).
8. S. Chaitanya Kumar, M. Ebrahim-Zadeh, "High-power, fiber-pumped, picosecond green source based on bismuth triborate", *Laser Phys.* 24, 025401 (2014).
9. V. Ramaiah-Badarla, A. Esteban-Martin, M. Ebrahim-Zadeh, "Two-crystal, synchronously-pumped, femtosecond optical parametric oscillator", *Opt. Lett.* 40, 324-327 (2015).
10. S. Chaitanya Kumar, E. Sánchez Bautista, M. Ebrahim-Zadeh, "Stable, high-power, Yb-fiber-based, picosecond ultraviolet generation at 355 nm using BiB_3O_6", *Opt. Lett.* 40, 403-406 (2015).

Conference papers

1. **(Invited)** M. Ebrahim-Zadeh' "Optical Parametric Oscillators: Concepts, technology, applications", *International Commission for Optics (ICO-23)*, Santiago de Compostela, Spain, August 2014
2. **(Invited)** M. Ebrahim-Zadeh, "Optical parametric oscillators: New frontiers", *Photonics North*, Montreal, Canada, May 2014
3. **(Invited)** S. Chaitanya Kumar, M. Ebrahim-Zadeh, "Nonlinear photonics: Tunable sources from IR to UV", *International Conference on Optics and Optoelectronics* (*ICOL-2014)*, Dehradun, India, March 2014
4. **(Post-deadline)** V. Ramaiah-Bardarla, A. Esteban-Martin, S. Chaitanya Kumar, K. Devi, K. Zawilski, P. Schunemann, M. Ebrahim-Zadeh, "Ti:sapphire-pumped, deep-infrared, intra-cavity-cascaded femtosecond **optical parametric oscillator",** 6th EPS-QEOD Europhoton Conference, Neuchatel, Switzerland, August 2014
5. K. Devi, S. Chaitanya Kumar, M. Ebrahim-Zadeh, "Tunable, continuous-wave, single-frequency ultraviolet sources based on BiB_3O_6", Nonlinear Photonics, Barcelona, Spain, July 27-31, 2014
6. V. R. Badarla, A. Esteban-Martin, S. Chaitanya Kumar, K. Devi, K. T. Zawilski, P. G. Schunemann, M. Ebrahim-Zadeh, "$CdSiP_2$ optical parametric oscillator tunable across 6-8 μm synchronously pumped by a Ti:sapphire laser", Nonlinear Photonics, Barcelona, Spain, July 27-31, 2014
7. K. Devi, S. Chaitanya Kumar, M. Ebrahim-Zadeh, "FM Mode-Locked optical parametric oscillator: Pulse formation and spectral characteristics", CLEO, San Jose, USA, June 2014.
8. S. Chaitanya Kumar, A. Esteban-Martin, T. Ideguchi, M. Yan, S. Holzner, T.W. Hänsch, N. Picqué, M. Ebrahim-Zadeh, "Few-cycle, broadband, mid-infrared parametric oscillator pumped by a 20-fs Ti:sapphire laser", CLEO, San Jose, USA, June 2014

9. V. Ramaiah Badarla, S. Chaitanya Kumar, M. Ebrahim-Zadeh, “Yb-fiber-laser-pumped, high-power, high-repetition-rate dual-wavelength picosecond optical parametric oscillator”, CLEO, San Jose, USA, June 2014.

10. S. Chaitanya Kumar, S. Ghavami Sabouri, A. Khorsandi, M. Ebrahim-Zadeh, “Thermal management in high-power continuous-wave second harmonic generation”, CLEO, San Jose, USA, June 2014

Patents

1. M. Ebrahim-Zadeh, S. C. Kumar, “Dual-wavelength optical parametric oscillator”, UK Patent, 1405555.2. (Filed on 27 March 2014).

2. M. Ebrahim-Zadeh, V. Ramaiah-Badarla, A. Esteban-Martin, S. Chaitanya Kumar, “Intracavity cascaded optical parametric oscillator”, EU Patent, PCT/EP2014/059018. (Filed on 02 May 2014).

Project Title:

Compact, high-power, fiber-laser-based coherent sources tunable in the mid-infrared and THz spectrum

(EOARD Award # FA8655-12-1-2128)

Progress Report, Year 1 (30 September 2013)

Majid Ebrahim-Zadeh[1,2]

[1] *ICFO-The Institute of Photonic Sciences, Mediterranean Technology Park, 08860 Castelldefels, Barcelona, Spain*
[2] *Institucio Catalana de Recerca i Estudis Avancats (ICREA), Passeig Lluis Companys 23, Barcelona 08010, Spain*

Tel: 0034-93 553 4047; Fax: 0034-93 553 4000
majid.ebrahim@icfo.es; www.icfo.es

Abstract

During the first year of the program, we have made substantial progress in the experimental development and theoretical analysis of dual-wavelength optical parametric oscillators (DW-OPOs) in two-crystal configurations, and operating in the near- and mid-infrared. The primary focus has been the generation of independently tunable signal-idler wavelength pairs, with the goal of exploiting the generated OPO radiation to achieve tunable THz radiation in the 0.3-10 THz spectral range using difference frequency mixing (DFM) in extracavity and intracavity pumping configurations. We have investigated DW-OPO devices in both continuous-wave (cw) and high-repetition-rate picosecond time-scales.

In cw operation, we developed a theoretical model to describe the behavior of a DW-OPO comprising two identical 30-mm-long MgO:sPPLT crystals in a bowtie ring cavity, pumped with a single solid-state pump laser. By solving the coupled-wave equations, we have been able to determine the maximum threshold reduction, parametric gain acceptance bandwidth, and closest possible attainable wavelength separation in arbitrary dual-wavelength generation in the cw DW-OPO, and confirm the findings of the theoretical model with experimental results. We have also experimentally verified the high-power performance of such a cw DW-OPO, where we have been able to generate a total output power of 6.5 W for 16.2 W of pump power. We have further verified coherent energy coupling between the intracavity resonant signal waves in the cw DW-OPO, resulting in Raman spectral lines.

In high-repetition-rate picosecond time-scale, we have developed a compact, fiber-laser-pumped picosecond DW-OPO at 160 MHz based on two MgO:PPLN crystals sharing the same cavity, using an Yb-fiber pump laser at 1064 nm. The two idler wavelengths were shown to be independently tunable in the mid-infrared across 3118-3393 nm, and could be arbitrarily tuned, even to degeneracy and beyond, irrespective of operating wavelength. The picosecond DW-OPO provided two signal and idler pulse trains and delivered as much as 1.5 W of average signal power from each arm at a total (signal plus idler) power extraction efficiency as high as 42%. The two output signal pulse trains had durations of ~18 ps and ~15.2 ps with Gaussian spatial quality, and exhibited passive power stability better than 3.6% rms over >5 hours. We also demonstrated temporal tailoring of the pulse trains from the DW-OPO by controlling the delay between the pump pulses at the input to the two MgO:PPLN crystals.

1. Continuous-wave, dual-wavelength OPO – Theory and experiment

1.1. Theoretical Analysis

In order to develop a theoretical model, we considered a generic configuration for the cw DW-OPO, as shown in Fig. 1. The OPO is arranged in a ring resonator with two crystals X_1 and X_2 of lengths L_1 and L_2, respectively, located at the two focii of the cavity. The OPO is a *singly-resonant oscillator* (*SRO*), where only the signal waves generated by the individual crystals are resonant inside the cavity. In the generic design of Fig. 1, the crystals X1 and X2 are pumped by two separate pump beams of power P_{p1} and P_{p2}, respectively, and exit the cavity in a single-pass. However, we can also consider the use of a single pump beam, P_{p1}, for both crystals X1 and X2, corresponding to the schemes used in earlier reports [1]. We consider z as the propagation direction, with the entrance and exit faces of the crystal X_1 designated as z_1 and z_2, respectively, and z_3 and z_4 as the entrance and exit of the crystal X_2, respectively.

Using the coupled-wave equations [2], we can then investigate the main operating features of the device including parametric gain enhancement, threshold reduction, and gain acceptance bandwidth under two different schemes characterized by different boundary conditions. We analyze two SRO configurations:

(a) *Dual-crystal SRO* (*D-SRO*), where crystals X1 and X2 are pumped by a single pump beam, P_{p1}, and the transmitted pump as well as the signal and idler fields generated by X1 are present at the input to X2.

(b) *Two-crystal SRO* (*T-SRO*), where X1 and X2 are pumped separately by P_{p1} and P_{p2}, respectively, and only the signal field generated by X1 as well as P_{p2} are present at the input to X2, with the idler generated by X1 exiting the cavity in a single pass.

In both cases, the signal field at the entrance of crystal X1 is finite, $A_{s1}(0)$, and the idler field at the entrance of X1 is zero, $A_{i1}(0)=0$. We neglect pump depletion and all signal losses due to the cavity mirrors. All results for D-SRO and T-SRO are compared to the conventional *single-crystal SRO* (*S-SRO*).

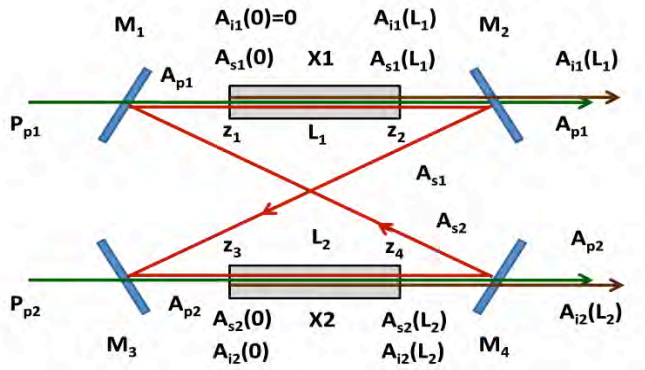

Fig. 1. Generic configuration of DW-OPO. Green, red and brown colors represent pump, signal and idler, respectively.

Parametric gain enhancement and gain acceptance bandwidth

Using the above generic configuration, and solving the coupled-wave equation in the undepleted pump approximation [2], we preformed numerical simulations to determine the parametric gain enhancement and acceptance bandwidths for D-SRO and T-SRO, and compare with the conventional S-SRO scheme [3]. For our simulations, we used the design parameters associated with a DW-OPO based on two identical 30-mm-long MgO:sPPLT crystals under temperature phase-matching and pumped at 532 nm [4].

The results of the simulations are shown in Fig. 2. At low gain (ΓL<<1), the parametric gain of D-SRO (red line) and T-SRO (blue line) are four-times and two-times that of the S-SRO (black line), respectively, under perfect phase-matching (ΔkL=0). On the other hand, comparing the gain acceptance bandwidths (FWHM), it is evident that the D-SRO has a gain bandwidth one-half of that of the S-SRO, whereas the gain bandwidth of T-SRO is equivalent to that of the S-SRO. Despite the reduced gain in the T-SRO as compared to D-SRO,

the wider gain bandwidth (larger temperature acceptance bandwidth) of T-SRO provides better tolerance to fluctuations in the crystal temperature, reducing the constraints on the stability of the oven and temperature controller without significant impact on the SRO output stability. At the same time, since the idler is completely transmitted after the first crystal in the T-SRO, it is not necessary to control the relative phases among the interacting waves at the entrance of the second crystal to maintain forward energy flow from the pump to the generated waves. The idler in the second crystal is generated from zero initial power and its phase is automatically adjusted to achieve highest parametric gain in the second crystal. Thus, the T-SRO has all the advantages of an S-SRO including wider gain bandwidth, higher output stability, no requirement of control of the input phases, and additionally higher parametric gain and lower operation threshold. The scheme is also generic and can be used for *N* number of crystals with proper cavity designs.

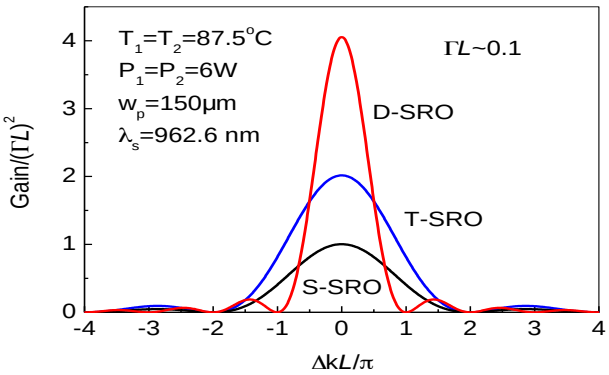

Fig. 2. Theoretically simulated normalized parametric gain of the S-SRO (black), D-SRO (red) and T-SRO (blue) as a function of phase-mismatch.

Effect of gain overlap in D-SRO and T-SRO

To study the effects of gain overlap in D-SRO and T-SRO, we calculated the gain for the two configurations as a function of signal wavelength, while maintaining crystal X1 at constant temperature (T1=91°C) and varying the temperature, T2, of crystal X2. The results are shown in Fig. 3. The temperature difference between the two crystals is defined as ΔT_{diff}=T1-T2. For comparison, we have also produced in Fig. 3 the gain variation of the S-SRO with signal wavelength at ΔT_{diff}=T1-T2=0. As can be seen from Fig. 3(a), the S-SRO (black curve) and T-SRO (blue curve) have a similar gain acceptance bandwidth ($\Delta\lambda_s\approx$1.3 nm), whereas D-SRO (red curve) has gain bandwidth one-half to that of the S-SRO. In the S-SRO, a small change in the crystal temperature from 91°C to 92°C shifts the gain maximum from 957.6 nm and 956.3 nm, resulting in a signal wavelength shift of $\Delta\lambda_{S\text{-}SRO}\approx$1.3 nm ($\Delta\nu_{S\text{-}SRO}$=0.42 THz), which is equal to the gain acceptance bandwidth ($\Delta\lambda_s\approx$1.3 nm) of the S-SRO, as shown by the black curves in Fig. 3(b). However, in the case of D-SRO, for the crystals at slightly different temperatures, T1=91°C and T2=92°C with ΔT_{diff}=1°C, ($\Delta k_1\neq\Delta k_2$, Δk_1=0, Δk_2=0), the gain of the individual crystals become overlapped, resulting in three main maxima in the D-SRO, each separated by ≈0.8 nm (red curve, Fig 3(b)). The two side maxima correspond to the individual crystal temperatures and the central maximum corresponds to the gain coupling between the crystals, resulting in a wider gain bandwidth of ≈2.1 nm. Consequently, the signal waves generated by the individual crystals in the D-SRO at a wavelength difference of $\Delta\lambda_{D\text{-}SRO}$ cannot be separated as long as $\Delta\lambda_{D\text{-}SRO}$ is much greater than the S-SRO gain bandwidth. The side maxima are also shifted by 0.1°C with respect to the main maximum in the S-SRO due to the influence of the secondary maxima of the S-SRO.

In case of T-SRO, however, the gain has two maxima corresponding to the individual crystal temperatures with a dip in between, indicating the possibility of operating the T-SRO with two closely spaced wavelengths with difference as small as the gain bandwidth of the individual crystals (S-SRO) without gain competition, as is the case in D-SRO. It is also to be noted that both maxima in the T-SRO gain profile exactly match the S-SRO maxima without any shift due to the secondary maxima of S-SRO, as is the case for the D-SRO. With further increase in the difference in crystal temperature, ΔT_{diff}=2°C (T1=91°C, T2=93°C), the gain of the individual crystals are completely separated in both D-SRO and T-SRO, as shown in Fig. 3(c), resulting in independent oscillation conditions for the two crystals, thus generating two distinct wavelengths. From this study, it is clear that the generation of two distinct wavelengths with separation, $\Delta\lambda$, can be possible if $\Delta\lambda$ is greater than (or equal to) the gain bandwidth of the individual crystals in the D-SRO (T-SRO) configuration.

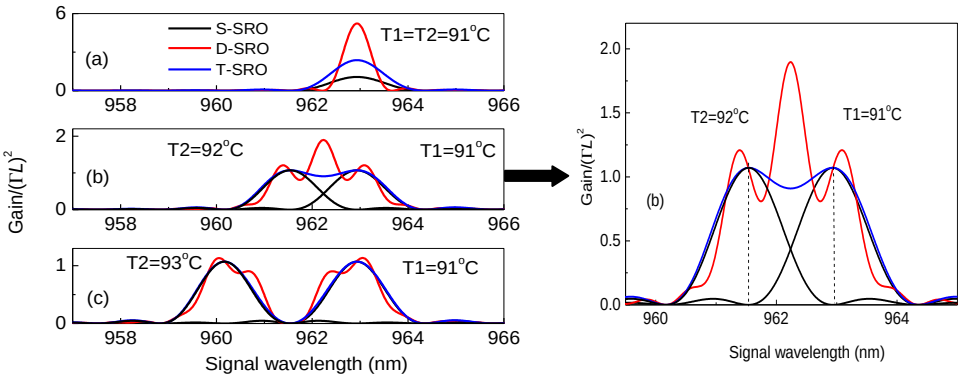

Fig. 3. Calculated gain of the S-SRO (black), D-SRO (red) and T-SRO (blue) versus signal wavelength at different combination of crystals' temperatures, (a) T1=T2=91°C, (b) T1=91°C, T2=92°C and (c) T1=91°C, T2=93°C. Fig (b) is zoomed in the right side for further clarity.

Based on the above simulation results, it is clear that the D-SRO has superior performance in terms of higher maximum gain and lower threshold than the T-SRO scheme, but is inferior with regard to gain bandwidth. However, as compared to T-SRO, the D-SRO suffers from disadvantages of cumulative thermal effects as well as optical damage in the individual crystals at higher pump powers, the requirement for the maintenance of constant relative phases among the interacting waves between the two crystals, and other limitations, as summarized in Table 1. Additionally, the pump depletion in the first crystal degrades the performance of the second crystal, making the D-SRO imbalanced when operating at two different wavelengths.

Because of its many advantages, we have focused on experimental studies on the T-SRO and have verified the performance of this scheme with regard to the various operating parameters derived in our calculations.

Table. 1. Comparative study of the D-SRO and T-SRO configurations

	D-SRO	**T-SRO**
Pump depletion	Depletion in X1 degrade the performance of X2	No effect, pumps are independent
Optimum pump focusing	Difficult in case of crystals located in series	Easily achieved, pumps are focused independently
Thermal dephasing	Accumulated along the length of the crystals	Distributed due to the independent pumping
High power operation	Restricted, crystal damage at high pump power	Possible, pumps are divided, no crystal damage
Relative phase	Need to maintain between the crystals	No need, new idler phase adjusts at each crystal

1.2. Experimental results and discussion

Experimental setup

The configuration of the two-crystal cw DW-OPO used in our experiments is shown in Fig. 4. The DW-OPO is configured in a T-SRO scheme comprising a compact symmetric ring cavity formed by four concave mirrors, M_1-M_4, of the same radius of curvature (r=10 cm) [4]. All mirrors are highly reflecting (R>99%) for the signal (890-1000 nm), while highly transmitting (T=75%-95%) for the idler (1100-1400 nm) and pump (T=97% at 532 nm). In the present study, we have used two identical 30-mm-long MgO:sPPLT nonlinear crystals (X_1 and X_2) containing a single grating period, Λ=7.97 μm. The crystals are housed in separate ovens with temperature stability of ±0.1°C. Due to different heating configurations [5,6] used for crystal X1 (closed-top) and X2 (open-top), the crystals have a temperature offset of ~2.5°C (T1=T2-2.5°C, where T1 and T2 are the temperatures of crystal X1 and X2, respectively). The crystal faces are AR-coated for the signal (R<0.5%) and pump (R<0.5% at 532 nm), with varying transmission across the idler tuning range (T=85-99%). The crystals are pumped separately with P1 pumping X1 and P2 pumping X2. In the present experiment, we have used a single pump laser and divided into two pump beams, P1 and P2, using a beam-splitter. The input powers to X1 and X2 are controlled using two separate power attenuators comprising a

half-wave-plate (λ/2) and a polarizing beam-splitter cube (PB1 for X1 and PB2 for X2). The second half-wave-plate (λ/2) in each pumping arm is used to yield the correct input polarization for phase-matching. Using two identical lenses, L1 and L2 (f=15 cm), the pump beams are focused to the same beam radius of w_{op}~31 μm at the center of X_1 and X_2 [7], corresponding to a focusing parameter, ξ=1 [8]. The focusing parameter is defined as $\xi=l/b_p$, where l is the length of the crystal, and $b_p=kw_{op}^2$ is the confocal parameter of the pump, with $k=2\pi n_p/\lambda_p$, where n_p, λ_p, and w_{op} are the refractive index, wavelength, and waist radius of the pump beam inside the crystal, respectively. The T-SRO cavity provides a signal beam waist w_{os}~41 μm at 900 nm, resulting in optimum spatial overlap in both crystals ($b_s=b_p$) [7]. Both mirrors, M_2 and M_4, transmit the pump and idler radiation generated in the respective crystals, X1 and X2. The output idler beams are separated from the residual pump and the leaked signal beams using the mirrors, M_5. The total optical length of the cavity is 56 cm, corresponding to a free-spectral range of 535 MHz. The fundamental pump source is a 10 W, frequency-doubled, cw diode-pumped Nd:YVO_4 laser at 532 nm [3].

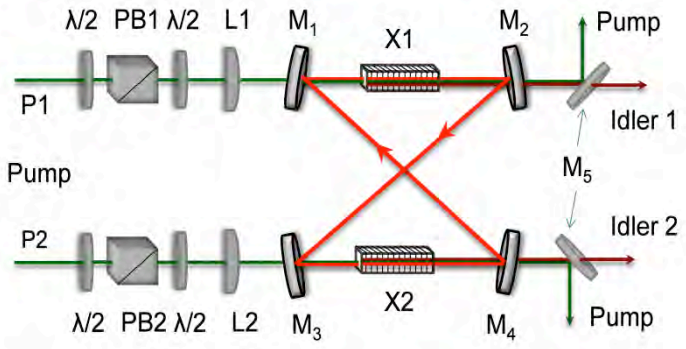

Fig. 4. Experimental design of the cw T-SRO. λ/2, half-wave plate; PB1-2, polarizing beam-splitter; L1-2, lens; M, mirror; X1-2, MgO:sPPLT crystal in oven. P1-2, pump power to the crystals X1-2. The pump beam can be from the same laser or from two different lasers.

Generation of dual-wavelengths with closest possible proximity

To compare our theoretical calculations with measurements, we reproduced the experimental results on the closest possible pair of distinct resonant signal wavelengths obtained previously [4]. In the experiment, we varied the crystal temperatures towards each other, while recording the distinct wavelengths. The results are shown in Fig. 5. At T1=90°C and T2=94°C, two distinct signal wavelengths with a separation, Δλ~1.76 nm, corresponding to a frequency difference, Δν~0.55 THz, were obtained.

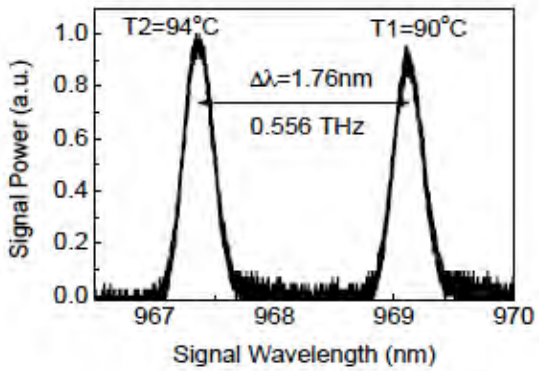

Fig. 5. Closest possible proximity of the dual signal wavelengths generated by the two crystals in T-SRO configuration.

The wavelength separation between the two distinct signal outputs is greater than the spectral acceptance bandwidth (~1.3 nm) of the 30-mm-long MgO:sPPLT crystals. Further variation in the crystal temperatures produces gain overlap of the two SROs, thus resulting in a single resonant wavelength. By reducing the spectral acceptance bandwidth of the MgO:sPPLT crystal, one can in principle generate two distinct signals with frequency difference below 0.55 THz. This can be achieved by using longer crystals (currently limited to 30 mm), or by operating the two SROs far from degeneracy, where the signal wavelengths have higher dispersion, thus resulting in narrower phase-matching bandwidth.

Generation of arbitrary dual-wavelengths

To verify the generation of dual-wavelength radiation with arbitrary values, we adjusted the individual crystal temperatures and measure the signal wavelengths from the two crystals. The results are shown in Fig. 6. To compare the theoretical predictions with experimental measurements, we have reproduced earlier results reported previously [4].

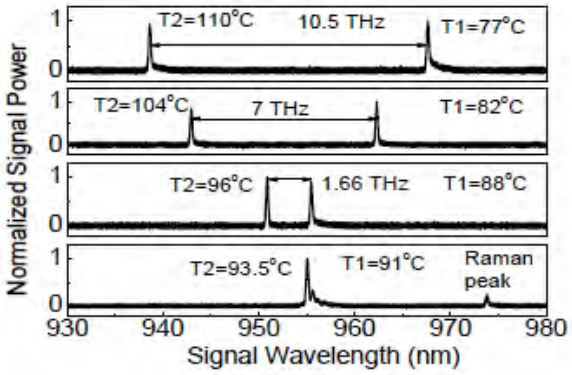

Fig. 6. Signal spectra of the two crystals X1 and X2 of the T-SRO for different combinations of their temperatures (T1, T2). Both the crystals are pumped with equal pump powers P1=P2=5W.

For dual-wavelength generation, we operated the T-SRO by pumping both crystals with equal input powers (~5 W), well above the S-SRO threshold, so that each crystal can operate as an independent S-SRO. As a result, at T1=77°C and T2=110°C, the T-SRO generates two resonant signal waves at 939.4 nm and 971.4 nm (idler at 1226.7 nm and 1176.1 nm, respectively) with a frequency difference of 10.5 THz. If we increase T1 and decrease T2, for different combinations of (T1, T2) resonant signal waves with frequency difference of 7 THz (82°C, 104°C) and 1.66 THz (88°C, 96°C) are generated. Further increase in T1 to 91°C and decrease in T2 to 93.5°C results in both crystals generating a single wavelength (955 nm), but with an additional spectral component with a wavelength shift of ~17 nm (~204 cm^{-1}) [9] from the resonant signal wavelength, which is attributed to stimulated Raman emission.

C***oherent energy coupling and Raman effect***

Typically, the stimulated Raman lines appear at intracavity powers greater than the Raman threshold power. When both crystals are operating away from each other, there is no evidence of the additional spectral components, since the intracavity power of each of the two circulating signal waves at a given pump power is below the Raman threshold power. Once both the crystals operate at the same signal wavelength, coherent-coupling between the resonant signal waves increases the total intracavity power, leading to the generation of Raman lines. Under coherent energy coupling, the signal generated by one crystal is amplified in the other crystal in presence of the pump power, and vice versa, resulting in an increase of the overall signal power. In this case, the T-SRO behaves as an S-SRO with a crystal length equal to the sum of the lengths of the two crystals. If the pump beam to one crystal is blocked, the other crystal still operates, maintaining OPO oscillation. However, in this case, there was no signature of additional spectral lines despite the longer total crystal length. To verify coherent energy coupling between the signal waves generated by the two crystals, we pumped X1 with a power of P1=5.2 W, while pumping X2 with a power of P2=1 W, and measured the signal spectra. The results are shown in Fig. 7. When P1 to crystal X1 is blocked, no oscillation is observed, since P2 to crystal X2 is well below the S-SRO threshold. On the other hand, when we block P2 to X2, crystal X1 still generates signal and idler radiation, since the pump power to X1 is well above the S-SRO threshold. However, we did not observe any additional spectral lines, which can be attributed to insufficient intracavity power. When both pump beams are unblocked, we observe signal spectra with additional peaks at different sets of temperatures (T1, T2) for the two crystals, as shown in Fig 7(a) and Fig 7(b). Although the individual crystals cannot generate additional peaks when operating separately, when they oscillate simultaneously and under the same phase-matching condition, the signal radiation generated by X1 is amplified in X2, in the presence of P2, and vice versa. As a result, the total intracavity signal power increases from its initial value, thus generating the additional spectral peaks. This observation verifies coherent energy coupling in the T-SRO, which can is also confirmed by the threshold reduction effect reported earlier [4].

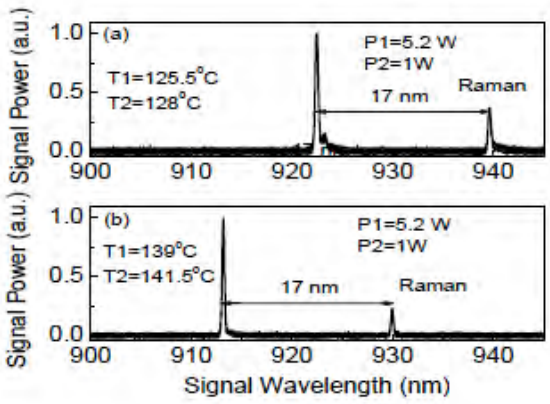

Fig. 7. Signal spectra of the T-SRO for different combinations crystal temperatures, (a) T1=125.5°C, T2=128°C and (b) T1=139°C, T2=141.5°C across the tuning range. Crystal X1 is pumped with power P1=5.2 W well above the threshold, while crystal X2 is pumped at P2=1 W well below threshold.

From Fig. 7(a) and Fig. 7(b), it is evident that for two different signal wavelengths of 922 nm (T1=125.5°C, T2=128°C) and 912 nm (T1=139°C, T2=141.5°C), and for any other signal wavelength across the entire SRO tuning range (850-1430 nm) [3], the additional spectral line is always red-shifted from the main signal peak by ~17 nm (~204 cm^{-1}), independent of the signal wavelength. This observation confirms that the additional spectral line is only due to the Raman effect, as the excitation of the phonon mode is the same for any excitation energy, and not due to the cascaded parametric process as reported for MgO:PPLN crystal [10]. The constant wavelength shift of ~17 nm (~204 cm^{-1}) is a characteristics of the medium, here the MgO:sPPLT crystal [9]. The difference in the crystal temperatures T1 and T2 to generate same wavelength is due to the difference in crystal heating configurations, as noted earlier.

Intracavity parametric amplification

We also studied the intracavity parametric amplification process in the T-SRO. The results of this study are shown in Fig. 8. In the experiments, crystal X1 is pumped with a power of P1=5W, above the S-SRO threshold. The generated idler is transmitted through the output mirror, M_2 (see Fig. 4), while the signal radiation seeds the crystal X2. In the absence of any pump power to X2, no idler power is present at the output mirror, M_4. However, increasing the pump power to X2 from zero, and under the same phase-matching condition as X1, the idler power generated by X2 rises linearly with the pump power, P2. At crystal temperatures of T1=77.5°C and T2=80°C (corresponding signal at λ_s=972 nm, idler at λ_i=1175.5 nm), the idler power measured at the output of mirror M_4 increases from zero to a maximum of 1.5 W at the highest available pump power of P2=4.5 W. The slope efficiency is 33.3% and there is no sign of saturation. Similarly at other crystal temperatures, T1=192°C and T2=194.5°C (λ_s=880 nm, λ_i=1345.2 nm) further away from degeneracy, a maximum idler power of 1.2 W is generated for a pump power of P2=4.25 W at slope efficiency of 26.4%. The reduction in the maximum idler power and slope efficiency is attributed to the reduction in the overall gain further away from degeneracy. The pump depletion in both the cases has a maximum of ~80%.

To verify the effect of seed signal power on the idler generation from X2, we measured the idler power generated by X2 as a function of the pump power, P2, for different signal seed powers. The results are shown in Fig. 9. For different pump powers, P1=4.5, 5.5, 6 and 6.5 W, to crystal X1, at T1=139°C, the intracavity signal power can be estimated from the leaked signal power out of one of the highly-reflecting mirrors (M1-M4) to be 55, 60, 70 and 78 W, respectively, although a precise estimate requires an output coupler. At each seed power, we varied the pump power, P2, and measured the idler slope efficiency, as shown in Fig. 9. The idler slope efficiency for the crystal X2 at T2=141.5°C was measured to be almost constant at ~25%, similar to our earlier report [11], irrespective of the signal seed power. As the seed power is already sufficiently high for all pump powers to X2, it has no effect on the slope efficiency of the idler. The effect of the seed on idler slope efficiency can become significant when the seed power is comparable to the input pump power, which can be the case when X1 is operated at threshold. Again the maximum pump depletion is ~80%

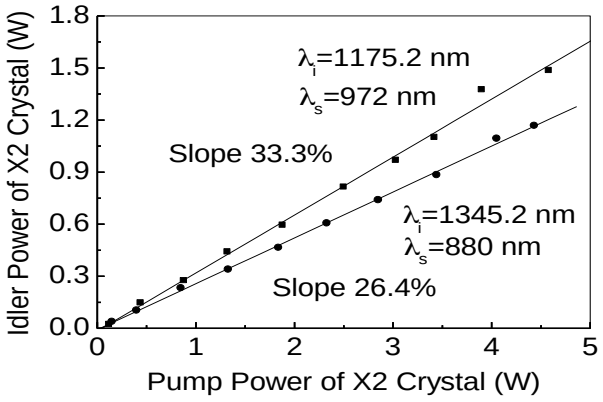

Fig. 8. Variation of Idler power of crystal X2 as a function of pump power across the tuning range with the seed from crystal X1.

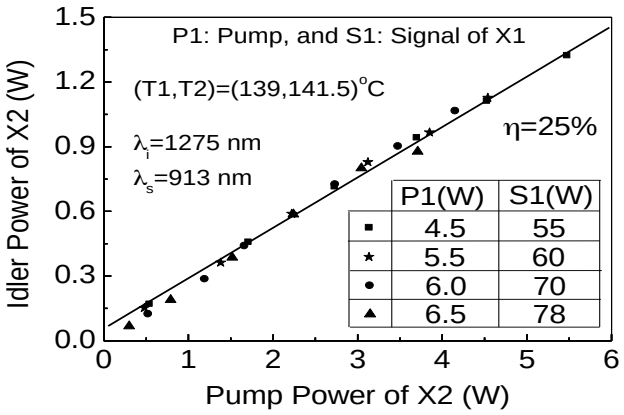

Fig. 9. Variation of idler power generated by X2 as a function of pump power for different intracavity signal seed powers. The crystal temperatures are T1=139°C, T2=141.5°C, corresponding to signal (idler) wavelength of 913 nm (1275 nm).

Threshold reduction

Intracavity parametric amplification and the appearance of stimulated Raman spectral lines verify coherent energy coupling in the T-SRO when the two crystals are operating under the same phase-matching condition. This will, in turn, reduce the T-SRO operation threshold, as also predicted in the theoretical analysis of this scheme [12]. To compare the threshold reduction estimated by theoretical analysis with experimental results, we have reproduced the power scaling for both the S-SRO and T-SRO in Fig. 10. For the T-SRO, both crystals were pumped at equal powers, whereas for the S-SRO one crystal was pumped while the other crystal was kept inside the cavity on purpose to obtain similar cavity mode condition as the T-SRO. At crystal temperatures, T1 = 91°C and T2 = 93.5°C, the S-SRO has a threshold of 3.17 W, slightly higher than our previous report [7], attributed to the additional loss due to the coating of the second crystal. The maximum total output power of the S-SRO (idler plus leaked-out signal) is >2.52 W for a pump power of >9.5 W. The output power is nearly saturated at higher pump powers due to the thermal effects, as discussed in our earlier report [11]. We observed Raman peak at a pump power of 7.4 W. In case of T-SRO, we have twice the crystal length than S-SRO, and hence intuitively expect a 75% reduction in threshold. However, the T-SRO has an operating threshold of 1.94 W, representing a 39% threshold reduction with respect to S-SRO, and has a higher total output power (>2.81 W) without any sign of saturation. In the T-SRO, the signal of one crystal is amplified in the other crystal and the idler is completely transmitted after each crystal, resulting in partial reduction in operational threshold. However, the sacrifice in the optimum threshold reduction (75%) is compensated by the less concomitant difficulties in resonating both the signal and idler in the same cavity, in addition to preserving the relative phases among the interacting waves from one crystal to the other as

necessary in the D-SRO. Moreover, the generated idler waves in the T-SRO automatically adjust their phase depending on the initial phases of the pump and signal at the input to each crystal, thus avoiding the need for phase control elements.

It can also be seen from Fig. 10 that the Raman shift appears at lower pump power (6.1 W) as compared to the S-SRO. The threshold reduction and the appearance of Raman peak at lower pump power confirm coherent coupling between the resonant signals of the individual crystals and the T-SRO behaves as a S-SRO with longer crystal length. In addition, the distribution of pump power reduces thermal effects and potential damage to the crystals, while improving the overall performance of the SRO in terms of higher output power and lower operation threshold. The T-SRO scheme thus offers the possibility of operation at relatively high pump powers (>10 W), where crystal damage is a major challenge to overcome. The lower threshold reduction (39%) from S-SRO to T-SRO in Fig. 10, compared to the theoretically estimated value (50%) can be attributed to imperfect mode overlap, crystal absorption and coating loss.

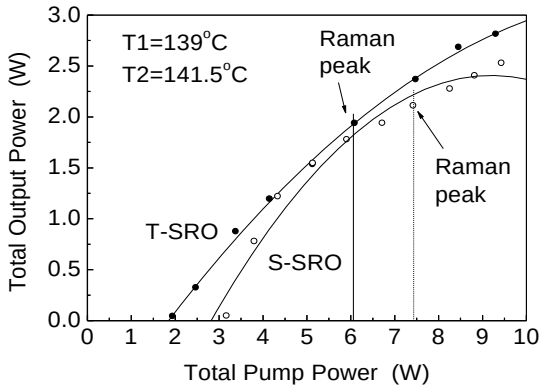

Fig. 10. Power scaling of the T-SRO and S-SRO as a function of total input pump powers for crystal temperatures T=139°C and T2=141.5°C corresponding to signal (idler) wavelength 913 nm (1275 nm). Solid curves are guide to the eye.

Power scaling and high power operation of the T-SRO

To verify the performance of the T-SRO at higher pump powers, we measured the total output power as a function of the input power >10 W, with the results shown in Fig. 11. To extract the signal radiation, we set the crystal temperatures at T1=70.5°C and T2=73°C, corresponding to a signal (idler) wavelength of 980 nm (1163.7 nm), where both the mirrors, M_2 and M_4, have a small transmission of 0.4% at the signal wavelength. At other signal wavelengths, all mirrors have reflectivity of >99.9%. As evident from Fig. 11, the S-SRO output power saturates at higher pump powers (>10 W), and roll-off in the pump depletion occurs, as reported earlier [7], due to the thermal effect arising from the higher pump powers. Using a green laser of maximum power 18 W, we further increased the pump power to the S-SRO and measured the idler output power. The idler power increases with the pump power in a similar manner to the results shown in Fig. 10. However, for pump powers beyond 10 W, we observe crystal damage. In repeated trials, we have observed similar bulk damage in the crystal, which can be attributed to thermal effects arising from the focusing of the high pump power into a small beam waist radius (w_0~30 μm) at the center of the crystal. Such crystal damage places an upper limit to the input pump power for the S-SRO under the given experimental conditions of ~10 W. We, however, expect that high-power operation of the S-SRO can be obtained using loose focusing, but at the expense of increased threshold. On the other hand, since in the T-SRO we divide the input power into two crystals, the pump power in each crystal is below the damage threshold, even for a total input power of 18 W. As evident from Fig. 11, the total output power of the T-SRO (the sum of the powers at the exit of mirror M_2 and M_4) increases with the increase in pump power at a slope efficiency of 40%, providing a maximum total power of 6.5 W for 16.2 W of pump power. The corresponding maximum signal and idler powers are 2.2 W and 4.3 W, respectively, which is the highest idler power ever reported using MgO:sPPLT crystal pumped in the green.

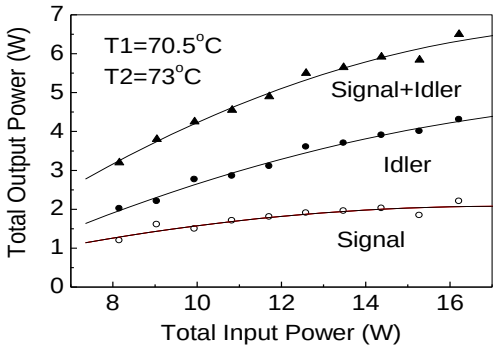

Fig. 11. Variation of total output power, out-coupled signal power and idler power of the T-SRO as a function of pump power at crystal temperatures T1=70.5°C and T2=73°C. Corresponding signal (idler) wavelength is 980 nm (1163.7 nm). Solid curves are guide to the eye.

It should also be noted that although in the T-SRO the thermal dephasing effect is also distributed with the division of the pump power into the two crystals, thermal effects arising from the higher intracavity power, as also reported earlier [11], can still be a major challenge to overcome. As also evident from the Fig. 11, the idler power increases with the pump power while there is no significant increase in the out-coupled signal power. The saturation of the intracavity signal power can be attributed to the thermal dephasing in the nonlinear crystals at higher intracavity power and can, in principle, be lowered by reducing the intracavity power using higher output coupling. The increase in operation threshold, due to higher output coupling and loose focusing of the pump beam to avoid crystal damage, can be compensated by the threshold reduction effect in the T-SRO. There is no evidence of saturation in the output power, indicating that the T-SRO can be operated at an even higher power. Given this potential, using a single output coupler for the signal, one could possibly extract sufficient signal power in a single signal beam for extracavity THz wave generation.

Power across the tuning range

We also measured the total output power as a function of the temperature T1 of crystal X1 across the tuning range, with the results shown in Fig. 12. For each value of T1, we adjusted T2 of crystal X2, so that both crystals were operating under coherent coupling condition at the same signal and idler wavelengths. At a total pump power of 16.2 W (with P1=P2=8.1 W), the total output from the T-SRO varies from 5.52 W at T1=64°C to 3.53 W at T1=127°C, with a maximum of 6.5 W at T1=70.5°C. The reduction in the total output for crystal temperatures away from degeneracy can be attributed to the reduced signal power (few milliwatts) due to the high reflectivity (R>99.9%) of the output mirrors, M_2 and M_4, higher reflection loss of the crystal coating, and the gain reduction factor [7]. Although we have measured the output power up to 127°C to verify the high power performance of the T-SRO without any crystal damage even at lower temperatures, one can in principle extend its operation across the entire tuning range of 850-1430 nm [3]. The pump depletion of both crystals varies by ~70-80% across the tuning range. The signal (idler) wavelength varies from 991 nm (1148.6 nm) to 916 nm (1269 nm) for a change in crystal temperature from 64°C to 127°C.

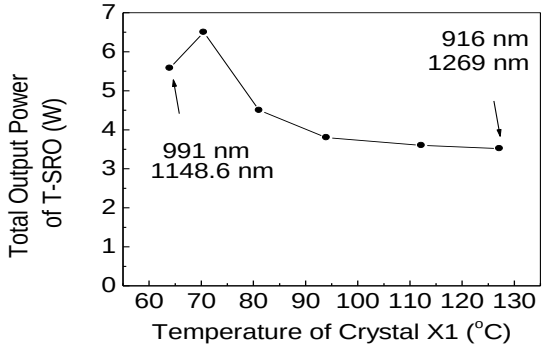

Fig. 12. Variation of total output power of the T-SRO across the tuning range (P1=P2=8.1 W). Solid curves are guide to the eye.

2. Fiber-laser-pumped, dual-wavelength picosecond OPO

We have also developed a picosecond dual-wavelength OPO (DW-OPO) based on two nearly identical nonlinear crystals sharing the same optical cavity, providing two independent and widely tunable pairs of singal-idler pulse trains across a wide tuning range of the device. The DW-OPO employs two MgO:PPLN crystals and is pumped by a mode-locked Yb-fiber laser, in a compact, robust, and practical architecture. The oscillator generates two pairs of signal-idler wavelengths that can be arbitrarily varied across the full tuning range of the OPO, even through degeneracy and beyond, irrespective of the operating wavelength.

Experimental setup

The schematic of the experimental setup is shown in Fig. 13. The pump source is mode-locked Yb-fiber laser at 1064 nm, providing up to 20 W of average power in 20 ps pulses at 80 MHz repetition rate. A Faraday isolator at the output end of the fiber protects the laser from any back- reflections. A combination of a polarizing beam-splitter and a half-wave-plate is used as a variable power divider, where the total available pump power is split into two arms in a controlled manner. A second half-wave-plate in each arm provides the required polarization for phase-matching in each crystal. The DW-OPO constitutes two synchronuously-pumped OPOs sharing the same optical cavity. The nonlinear gain media are two MgO-doped periodically poled lithium niobate (MgO:PPLN) crystals with identical grating periods ranging from Λ=28.5-31.5 μm in steps of 0.5 μm. However, in the present experiment, we only used a single grating period of Λ=30.5 μm. The pump beam in both the arms is focused using two lenses (L_1 and L_2) at the center of the respective nonlinear crystals to a beam waist radius of w_{o1}~w_{o2}~65 μm, corresponding to a confocal focusing parameter of ξ_1~ ξ_2~0.93 [8]. The DW-OPO resonator is configured in a folded ring cavity formed by four plano-concave mirrors (M_1–M_4) with radius of curvature (r=200 mm), a plane mirror (M_5) and an output coupler (OC). All mirrors (M_1-M_5) are highly reflecting (R>99%) over the signal wavelength range of 1.3–2.2 μm, and highly transmitting for the pump (T>90%) at 1064 nm and idler (T>87%) over 2.2–4 μm, ensuring singly resonant signal oscillation in both OPOs. A plane OC with partial transmission (T~20%) over 1100–1630 nm is used to extract the signal power from the DW-OPO and a dichroic mirror, M, separates the generated idler from the pump.

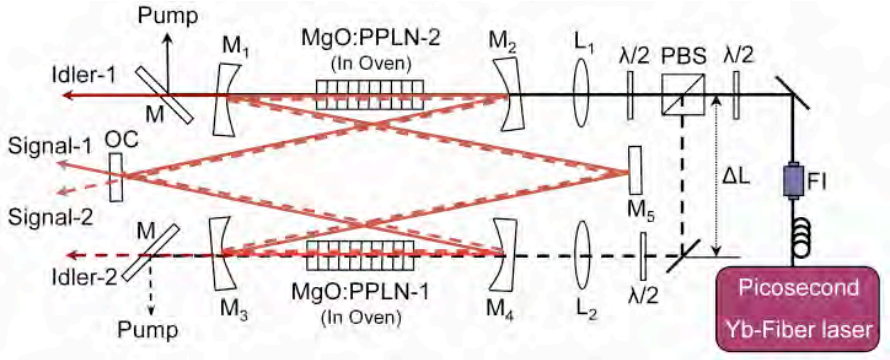

Fig. 13. Schematic of the picosecond Yb-fiber laser pumped dual-wavelength OPO. FI: Faraday isolator; λ2: Half-wave-plate; PBS: Polarizing beam-splitter; $L_{1,2}$: Lens; M: Mirrors; OC: Output coupler.

While a 48-mm-long, MgO:PPLN-1 serves as the nonlinear gain medium for OPO-1, a 50-mm-long MgO:PPLN-2 provides the gain for OPO-2. Both nonlinear crystals are housed in two identical ovens whose temperatures can be controlled from room temperature to 200ºC with a temperature stability of ±0.1ºC. The total optical length of the DW-OPO ring cavity is ~186 cm, corresponding to a repetition rate of 160 MHz, ensuring synchronization with the second harmonic of the pump laser repetition rate. It is to be noted that the pump pulses travel an additional path length of ΔL~43 cm, corresponding to a temporal delay of ~1.4 ns before entering OPO-2. Since, the two OPOs share the same optical cavity, the resonant signal pulses traverse through both nonlinear gain media in each round trip. However, due the temporal delay between the two input pump pulse trains, the generated signal pulses arrive at different times in each MgO:PPLN crystal, hence avoiding any possibility of coupling between the two OPOs, irrespective of the operating wavelengths. Further, the DW-OPO cavity is different from our earlier work in the cw [4] as well as femtosecond [13] time-scales. It is designed in such a way that the two OPOs are pumped through different arms and the corresponding signal pulses travel in opposite direction, again avoiding any coherent coupling, even when the resonant wavelengths

are significantly close and $\Delta L \sim 0$ or integral multiple of the length corresponding to repetition rate of the pump laser. Moreover, the counter-propagating signal pulses result in the signal output from the OC in different direction, enabling us to monitor the out-coupled signal from each OPO separately.

Results and discussion

In order to characterize the picosecond DW-OPO, we initially performed wavelength tuning by varying the temperature of each nonlinear crystals individually, enabling arbitrary tuning of two independent signal-idler wavelength pairs generated by the two crystals. Since coherent coupling is completely avoided in the present cavity design, the signal-idler pairs from the two OPOs can be tuned indefinitely far or infinitesimally close, even through degeneracy and beyond, irrespective of the operating wavelength. At a fixed pump power of 8 W for each OPO, the DW-OPO tuning behaviour is shown in Fig. 14. By fixing the MgO:PPLN crystal in OPO-2 at a temperature of T2=50 ºC, generating a signal wavelength of 1550 nm, and varying the temperature of MgO:PPLN crystal in OPO-1 from 150ºC down to 50ºC, the signal wavelength from OPO-1 could be continuously tuned from 1615 to1551 nm, reaching a degenerate point where both OPOs operate at nearly similar wavelengths. The signal wavelength is measured using a spectrometer (Ocean Optics, NIR Quest). The difference of 1 nm in peak wavelength between the two OPOs, while operating at the same temperature, could be attributed to a small delay in the cavity length due to the 2-mm difference in the length for the two MgO:PPLN crystals. It is to be noted the cavity of the DW-OPO is always optimized to achieve maximum output power. We also adjusted T1 slightly below 50ºC in order to operate at exact degeneracy, and observed no coherent coupling or perturbation between the two OPOs, even at the degenerate point of 1550 nm. Further, by adjusting T1 and T2, the degenerate point of operation can be shifted arbitrarily within the full tuning range of the OPO, making it a highly attractive and viable source for applications such as tunable THz generation.

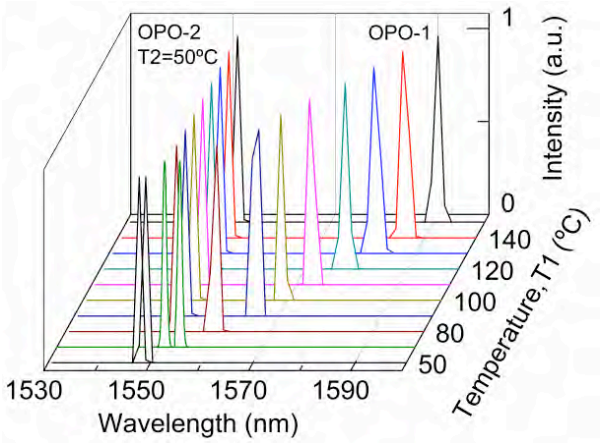

Fig. 14. Dual-wavelength tuning of the picosecond synchronously pumped DW-OPO

The output power of the picosecond DW-OPO across the signal tuning range from OPO-1 and OPO-2, for a fixed grating period of Λ=30.5 μm and a constant pump power of 8 W at the input to each OPO is shown in Fig. 15(a). The open circles correspond to the signal power extracted through the 20% OC from OPO-1, while solid circles correspond to the power from OPO-2. As evident from Fig. 15(a), the signal power from both OPOs remains almost constant at 1.35 W over the entire tuning range of 1550-1615 nm. The corresponding variation in the signal wavelengths as a function of temperature of the respective MgO:PPLN crystals is shown in Fig. 15(b). As can be seen, the two signal wavelengths generated from the OPO-1 and OPO-2 are almost identical in absolute value as well as tuning behavior. The dashed line in Fig. 15(b) corresponds to the theoretically calculated signal wavelength as a function of temperature (T1=T2) for a fixed MgO:PPLN grating period of Λ=30.5 μm, using the relevant Sellemier equations [14].

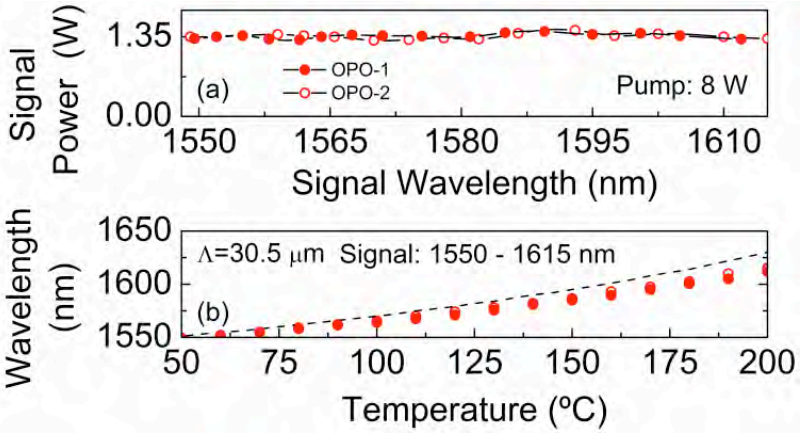

Fig. 15(a). Power across the signal tuning range, (b) signal wavelength as a function of temperature in the picosecond DW-OPO.

We also performed simultaneous power scaling measurements of the signal output extracted through the 20% OC, as well as the idler, as function of the input pump power to each OPO, with the results shown in Fig. 16. With both OPO-1 and OPO-2 operating at a constant temperature of T1~T2~50ºC, for a fixed grating period Λ=30.5 μm, corresponding to a signal wavelength of 1550 nm, we were able to extract as much as 1.35 W of average signal power from each OPO at 160 MHz, with a slope efficiency of ~18%, for a maximum available pump power of 8 W to each crystal at 80 MHz repetition rate, as shown in Fig. 16(a). The corresponding idler power is recorded to be 290 mW at a slope efficiency of ~3.8% at 3393 nm, as shown in Fig. 16(b). This corresponds to an overall extraction efficiency as high as 42% for the picosecond DW-OPO. There is no evidence of saturation in the extracted signal and idler power, indicating the possibility of further power scaling by increasing the input pump power. Moreover, optimization and fine-adjustment of signal output coupling can lead to further improvements in the output power [15]. Both OPO-1 and OPO-2 have a similar threshold, which is recorded to be <830 mW. Although the resonant signal wavelength is the same in both the OPOs, no threshold reduction is observed due to the lack of coherent coupling between the two OPOs, as observed in the cw DW-OPO [4].

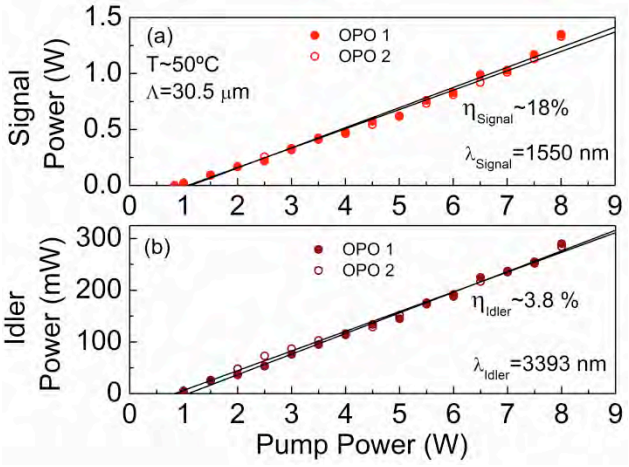

Fig. 16. Signal and (b) idler power scaling as a function of the pump power from the picosecond DW-OPO.

The long-term power stability measurement of the signal extracted from the each arm of the DW-OPO along with the spatial beam profiles at operating signal wavelengths near 1550 nm is shown in Fig. 17. The OPO-1 and OPO-2 are recorded to exhibit a passive power stability better than 2.2% rms and 3.6% rms, respectively, over >5 hours under free-running conditions, as shown in Fig. 17(a) and 17(b). The corresponding spatial beam profiles are shown in Fig. 17(c) and 5(d) for OPO-1 and OPO-2, respectively, confirming a single-peak Gaussian intensity distribution.

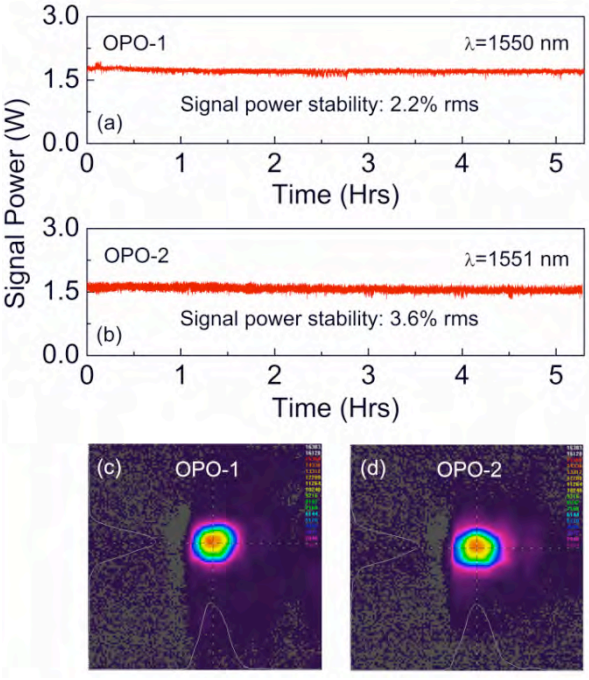

Fig. 17. Power stability of the signal extracted from (a) OPO-1 and (b) OPO-2. Spatial beam profile of the output signal from (c) OPO-1 and (d) OPO-2.

We also performed spectral and temporal characterization of the signal pulses from the DW-OPO, with OPO-1 and OPO-2 operating at different temperatures of T1=50 ºC and T2=100 ºC. The signal pulse duration was measured using a home-made interferometric autocorrelator based on a two photon-absorption Si photodetector. The results are shown in Fig. 18. The signal pulses from OPO-1 and OPO-2 were both recorded to have a Gaussian tempral width of ~18 ps and 15.2 ps, respectively. The pulse durations are conssitent, with the samll difference due to the different operating wavelegnths and crystal lengths . The corresponding spectra are shown in the inset of Fig. 18 centered around 1550 nm and 1569 nm, respectively. The spectra have smooth clean profiles with a FWHM bandwidths of X nm and Y nm for OPO-1 and OPO-2, repectively.

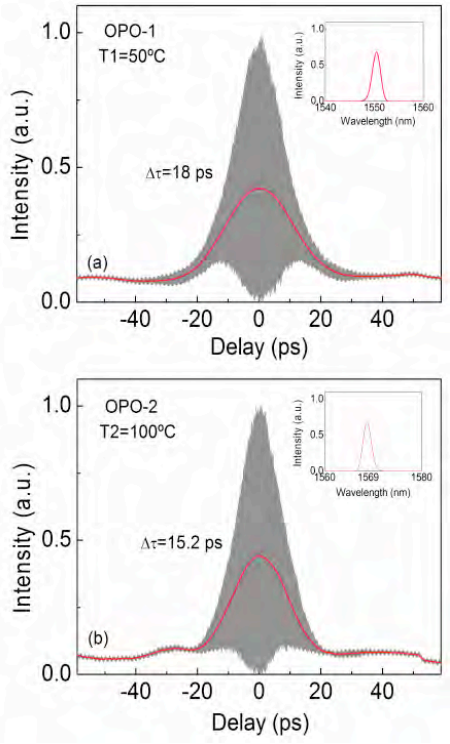

Fig. 18. Interferometric autocorrelation of the signal pulses from (a) OPO-1 and (b) OPO-2. Inset: Signal spectrum.

Finally, we measured the time delay between the two oscillating signal pulses by performing simultaneous measurements of the two signal pulse trains emitted from the DW-OPO using an InGaAs photodetector (20 GHz, 18.5 ps) and a fast oscilloscope (3.5 GHz, 40 GS/s). The result is shown in Fig. 19, where it is evident that the pulse in each train are separated by 6.3 ns, corresponding to a repetition frequency of ~160 MHz, while the two interleaved pulse trains from OPO-1 and OPO-2 are seperated by 1.4 ns, which corresponds exactly to the spatial delay of ΔL~43 cm between the pump pulses arriving at the input to OPO-1 and OPO-2, as shown in Fig. 13. Hence, another advantage of this configuration is that, by changing the delay between the input pump pulses, the signal pulses can be adjusted to operate at the desired time delay, maintaining the repetetion frequency of the individual pulse train at the same cavity length, yet avoiding any coherent coupling between the two signal wavelengths resonating inside the same cavity. Alternatively, with a fixed delay between the input pump pulses, the output signal pulse trains from the DW-OPO can be synchronized using an external delay line, which would enable single-pass frequency mixing in suitable nonlinear crystals to access new wavelegnths regions, with potential applications for THz generation using DFM.

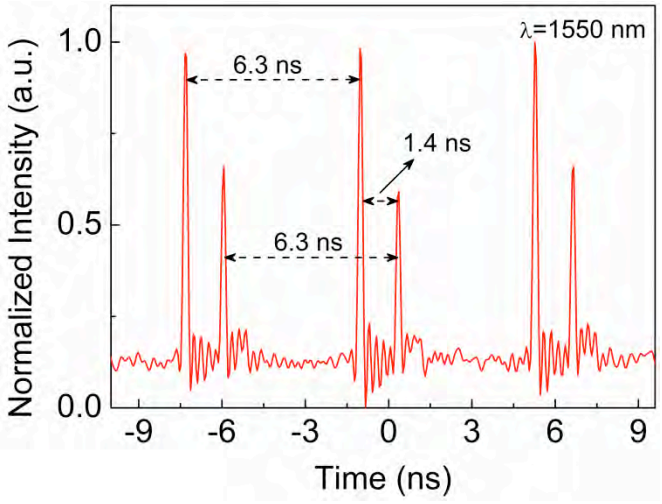

Fig. 19. Signal pulse train from the picosecond DW-OPO.

Conclusions and Summary

In conclusion, we have successfully developed a new class of cw and picosecond DW-OPO systems for the near- and mid-infrared in compact and practical architectures using solid-state and fiber pump lasers. We have performed theoretical modeling of experimental characterization of the developed OPOs with regard to the most important operating parameters including tunable wavelength coverage, oscillation threshold, output power and efficiency, spatial beam quality and stability.

In cw operation, by solving the coupled wave equations, we calculated the maximum threshold reduction of 50%, temperature acceptance bandwidth (FWHM) of 0.9°C, 0.8°C and 0.7°C at crystal temperatures 87.5°C, 139°C and 192°C, respectively, and closest possible arbitrary dual-wave generation with a wavelength separation of 1.39 nm at 91°C. We have measured a lower threshold reduction of 39% compared to the theoretically predicted value, which can be attributed to the additional losses due to the crystal coating, and material absorption. Although the T-SRO has two identical crystals, the parametric gain in this DW-OPO has an acceptance bandwidth equivalent to a single crystal. Experimentally, the closest signal wavelength (frequency) separation under arbitrary dual-wavelength operation has been observed to be 1.76 nm (0.55 THz), which also verifies the broadening of the temperature acceptance bandwidth. Due to the division of pump in two crystals, the T-SRO can tolerate a higher total pump power, reducing the risk of optical damage and thermal loading in the crystal. We also experimentally verified the high power performance of such scheme, where we obtained a total output power of 6.5 W for 16.2 W of green power at 532 nm. The intracavity parametric amplification of the resonant signal of one crystal in the other crystal shows the possibility of using different combinations of crystals and pump radiation. We verified the coherent energy coupling between the intracavity resonant signal fields resulting Raman spectral emission.

In the picosecond time-scale, we demonstrated a simple, compact, picosecond DW-OPO at 160 MHz repetition rate based on two MgO:PPLN crystals in a single cavity, synchronously pumped by an Yb-fiber laser at 80 MHz. The DW-OPO provides two signal and idler pulse trains, which are independently and arbitrarily tunable in the near-infrared across 1550-1615 nm, corresponding to the mid-infrared tunability over 3118-3393 nm, using a single grating period. The signal and idler can be tuned through any degenerate wavelength across the tuning range of the DW-OPO without coherent coupling. The wavelength coverage of the signal and idler pairs can be readily extended using multiple grating periods of the MgO:PPLN crystals. Moreover, we were able to extract signal power of up to 1.5 W from each OPO, at a total (signal plus idler) extraction efficiency as mush as 42%, with a power stability better than 3.6% rms over >5 hours in excellent spatial beam quality. Interferometric autocorrelation measurements resulted in Gaussian pulse duration of ~18 ps from OPO-1 and ~15.2 ps from OPO-2. The cavity design ensures no coherent coupling between the signal (idler) wavelength pairs, irrespective of the operating wavelength, while enabling degenerate operation at any desired wavelength across the tuning range of the DW-OPO. Further, by adjusting the delay between the pump pulses through an external delay line at the input to the two crystals, the delay between the pulse train from the DW-OPO can be tailored. The generic design can also be extended to new wavelength regions using alternative nonlinear materials and pump wavelengths. These characteristics make the described fiber-pumped DW-OPO a highly attractive and practical source of high-repetition-rate picosecond pulses for many applications, in particular tunable THz generation in the 0.3-10 THz range by exploiting extracavity and intracavity DFM techniques.

References

1. M. Tang, H. Minamide, Y. Wang, T. Notake, S. Ohno, and H. Ito, "Dual-wavelength single-crystal double-pass KTP optical parametric oscillator and its application in THz wave generation," Opt. Lett. **35**, 1698-1700 (2010).
2. A. Yariv and P. Yeh, *Optical Waves in Crystals* (Wiley, 1984).
3. G. K. Samanta, G. R. Fayaz, Z. Sun, and M. Ebrahim-Zadeh, "High-power, continuous-wave, singly resonant optical parametric oscillator based on MgO:sPPLT," Opt. Lett. **32**, 400-402 (2007).
4. G. K. Samanta, and M. Ebrahim-Zadeh, "Dual-wavelength, two-crystal, continuous-wave optical parametric oscillator," Opt. Lett., **36**, 3033-3035 (2011).
5. S. Chaitanya Kumar, G. K. Samanta, and M. Ebrahim-Zadeh, "High-power, single-frequency, continuous-wave second-harmonic-generation of ytterbium fiber laser in PPKTP and MgO:sPPLT," Opt. Express **17**, 13711-13726 (2009).
6. S. Chaitanya Kumar, G. K. Samanta, Kavita Devi, and M. Ebrahim-Zadeh, "High-efficiency, multicrystal, single-pass, continuous-wave second harmonic generation," Opt. Express **19**, 11152-11169 (2011).
7. G. K. Samanta, G. R. Fayaz, and M. Ebrahim-Zadeh, "1.59 W, single-frequency, continuous-wave optical parametric oscillator based on MgO:sPPLT," Opt. Lett. **32**, 2623-2625 (2007).
8. G. D. Boyd and D .A. Kleinman, "Parametric interaction of focused Gaussian light beams," J. Appl. Phys., **39**, 3597-3639 (1968).
9. T-H. My, O. Robin, O. Mhibik, C. Drag, and F. Bretenaker, "Stimulated Raman scattering in an optical parametric oscillator based on periodically poled MgO-doped stoichiometric $LiTaO_3$," Opt. Express **17**, 5912-5918 (2009).
10. J. Kiessling, R. Sowade, I. Breunig, K. Buse, and V. Dierolf, "Cascaded optical parametric oscillations generating tunable terahertz waves in periodically-poled lithium niobate crystals," Opt. Express **17,** 87-91 (2009).
11. G. K. Samanta and M. Ebrahim-Zadeh, "Continuous-wave singly-resonant optical parametric oscillator with resonant wave coupling," Opt. Express **16**, 6883-6888 (2008).
12. G. K. Samanta, A. Aadhi, and M. Ebrahim-Zadeh, "Continuous-wave, two-crystal, singly-resonant optical parametric oscillator: Theory and experiment"," Opt. Express 21, 9520-9540 (2013).
13. A. Esteban-Martin, V. Ramaiah-Badarla, and M. Ebrahim-Zadeh," Dual-wavelength optical parametric oscillator using antiresonant ring interferometer" Laser Photonics Rev. 6, No. 5, L7–L11 (2012).
14. O. Paul, A. Quosig, T. Bauer, M. Nittmann, J. Bartschke, G. Anstett, J.A. L'Huillier, "Temperature-dependent Sellmeier equation in the MIR for the extraordinary refractive index of 5% MgO doped congruent $LiNbO_3$," Appl. Phys. B, Lasers Opt. 86, 111 (2007).
15. S. Chaitanya Kumar, A. Esteban-Martin, and M. Ebrahim-Zadeh, "Interferometric output coupling of ring optical oscillators," Opt. Lett. 36, 1068-1070 (2011).

Publications:

Since the start of the project in September 2012, we have generated the following publications, with due acknowledgement to EOARD for their valuable support:

Journal papers

- G. K. Samanta, A. Aadhi, M. Ebrahim-Zadeh, "Continuous-wave, two-crystal, singly-resonant optical parametric oscillator: Theory and experiment", Opt. Express 21, 9520-9540 (2013).

- **(Invited)** M. Ebrahim-Zadeh, S. Chaitanya Kumar, A. Esteban-Martin, G. K. Samanta, "Breakthroughs in photonics 2012: Breakthroughs in optical parametric oscillators" IEEE Photon. J. 5, 0700105 (2013) - .

- V. Ramaiah-Badarla, A. Esteban-Martin, M. Ebrahim-Zadeh, "Self-phase-locked degenerate femtosecond optical parametric oscillator based on BiB_3O_6", Laser Photonics Rev. 7, L55–L60 (2013).

- K. Devi, S. Chaitanya Kumar, M. Ebrahim-Zadeh, Directly phase-modulation-mode-locked doubly-resonant optical parametric oscillator", Opt. Express 21, 23365-23375 (2013).

- O. Kimmelma, S. Chaitanya Kumar, A. Esteban-Martin, M. Ebrahim-Zadeh, "Multi-GHz picosecond optical parametric oscillator pumped by 80-MHz Yb-fiber laser, Opt. Lett. (2013) – In press.

- V. Ramaiah-Badarla, S. Chaitanya Kumar, and M. Ebrahim-Zadeh, "Fiber-laser-pumped, dual-wavelength picosecond optical parametric oscillator", Opt. Lett. (2013) – Submitted.

Conference papers

- G. K. Samanta, M. Ebrahim-Zadeh, "Theoretical and experimental study of two-crystal, continuous-wave, singly-resonant optical parametric oscillator, *NLO 50 International Symposium, Barcelona, Spain, October 2012*

- S. Chaitanya Kumar, O. Kimmelma, M. Ebrahim-Zadeh, "High-power, fiber-laser-pumped, tunable picosecond Source for the near-to-mid-Infrared", *The International Conference on Fiber Optics and Photonics*, IIT Madras, India, December 2012

- S. Chaitanya Kumar, O. Kimmelma, M. Ebrahim-Zadeh, "Novel trends in the development of picosecond near-infrared parametric sources", Winter meeting, *Condolider SAUUL*, Benasque, Spain, February 2013

- A. Esteban-Martin, V. Ramaiah-Badarla, M. Ebrahim-Zadeh, "Dual-wavelength synchronously-pumped femtosecond optical parametric oscillator using antiresonant ring interferometer", *CLEO/Europe-EQEC*, Munich, Germany, Paper: CD-5.3 MON, May 2013

- K. Devi, S. Chaitanya Kumar, M. Ebrahim-Zadeh, "Stable, continuous-wave, fiber-laser-based, ultraviolet generation in BiB_3O_6", *CLEO/Europe-EQEC*, Munich, Germany, Paper: CD-9.3 TUE, May 2013

- S. Chaitanya Kumar, G. K. Samantha, A. Adhi, M. Ebrahim-Zadeh, "Tunable fiber-laser-based picosecond source for the ultraviolet," *CLEO/Europe-EQEC*, Munich, Germany, Paper: CD-9.1 TUE, May 2013
